The surface interactions among iron oxides, humic substances, and biofilms

by Liwei Qi

A thesis submitted in partial fulfillment of the requirements for the degree of Master of Science in Chemical Engineering
Montana State University

Abstract:
The occurrence of biofilms in drinking water distribution systems has caused more and more water quality problems and become a major concern to the industry. It is known that iron pipe materials support more biofilms than other materials, and the effect is positively related to the corrosion potential of the materials. It is also known that iron oxide tends to accumulate natural organic carbon on its surface. The purpose of this thesis is to investigate the hypothesis that the adsorbed humic substances on iron oxide surface can serve as carbon and energy sources for biofilm cells to grow.

To study the relationship between iron oxide, adsorbed humic substances, and biofilms, an iron oxide surface was created on glass beads and glass coupons by slow hydrolysis and condensation reactions of a millimolar solution of iron nitrate in approximately 10-mM nitric acid at 70 °C. The physical, chemical, and mechanical properties of the surface were analyzed. The Elliot Silt Loam Soil humic substances were allowed to adsorb on the iron oxide surface in batch reactors. The adsorption isotherms at pH 6.7 and 7.4 were measured by TOC measurements. A desorption test was conducted to demonstrate the stability of the adsorbed humic substances. Four parallel plate flow cells with different coverslip surfaces were used for the biofilm growth studies. These coverslip surfaces included (1) glass, (2) iron oxide without pre-adsorbed humics, (3) iron oxide with pre-adsorbed humic of low surface coverage, and (4) iron oxide with pre-adsorbed humic of high surface coverage. A strain of Pseudomonas aeruginosa (PA01, GFP+) was chemostat cultured and inoculated into the flow cells. It was allowed to attach and grow on the coverslip surfaces. These cells produced fluorescence and were counted by real time microscopy. A TOC free medium and a 0.25-ppm C humic substance medium were allowed to flow through the flow cells in a laminar mode. The biofilm densities and accumulation rates of the different surface and media conditions were measured and compared.

The results of this study demonstrated that (1) the iron deposit method provided a proper iron oxide surface for the subsequent humic adsorption and biofilm growth research. (2) The created iron oxide surface had significant adsorption capacity and affinity to the Elliot Silt Loam Soil humic substances. The adsorption could be interpreted by the modified Langmuir adsorption isotherm with multiple-layer adsorption. The adsorption decreased with higher pH. The desorption process of the adsorbed humic substances was very insignificant and neglectable. (3) Neither the iron oxide nor the adsorbed humic substances alone could support significant biofilm accumulation on the surface. However, the adsorbed humic substances could be an additional nutrient to assist higher accumulation rate of the biofilm on the surface. The adsorbed humic substances also helped to attract and maintain more bacterial cells on the surface.

THE SURFACE INTERACTIONS AMONG IRON OXIDES, HUMIC SUBSTANCES, AND BIOFILMS

By

Liwei Qi

A thesis submitted in partial fulfillment
of the requirements for the degree

of

Master of Science

in

Chemical Engineering

MONTANA STATE UNIVERSITY-BOZEMAN
Bozeman, Montana

June, 1999

APPROVAL

Of a thesis submitted by

Liwei Qi

This thesis has been read by each member of the thesis committee and has been found to be satisfactory regarding content, English usage, format, citations, bibliographic style, and consistency, and is ready for submission to the College of Graduate Studies.

Dr. Anne K. Camper — Anne K. Camper (Signature) — 7/15/99 (Date)

Approved for the Department of Chemical Engineering

Dr. John T. Sears (Dept. Head) — John T. Sears (Signature) — 7/15/99 (Date)

Approved for the College of Graduate Studies

Dr. Bruce R. McLeod (Graduate Dean) — Bruce R. McLeod (Signature) — 7-21-99 (Date)

STATEMENT OF PERMISSION TO USE

In presenting this thesis in partial fulfillment of the requirements for a master's degree at Montana State University-Bozeman, I agree that the Library shall make it available to borrowers under rules of the Library.

If I have indicated my intention to copyright this thesis by including a copyright notice page, copying is allowed only for scholarly purposes, consistent with "fair use" as prescribed in the U. S. Copyright Law. Requests for permission for extended quotation from or reproduction of this thesis in whole or in parts may be granted only by the copyright holder.

Signature Liwei Qi

Date 7-15-99

ACKNOWLEDGEMENTS

It was a great pleasure to study and work in the Center for Biofilm Engineering, Montana State University, to develop my knowledge and skills. I would like to express my thanks to Anne Camper, who was the project leader and gave me extensive advice on the research; Calvin Abernathy, who shared his ideas about the relationship between corrosion products, humics and biofilms; Phil Butterfield and Chris Wend, who helped me with the TOC measurements; Ryan Jordan, who gave me information on the iron oxide coating method; Andy Rice, who shared the information of the bacteria and the microscopy method; and John Neuman, who helped me to arrange the laboratory work and equipment.

I would like to thank Marty Hamilton, who helped with the statistical analysis and interpretation; Ernie Visser, who did the MATLAB and bootstrap programming; and Fred Holdbreak, who did the statistical analysis of the biofilm growth data.

A special thank goes to John Sears and all the professors in the Chemical Engineering department who gave me great help on my education.

I wish to thank my parents who encouraged me to study abroad, and my wife, Lei, who gave me the happiest life for the last two years with love.

TABLE OF CONTENTS

LIST OF TABLES

LIST OF FIGURES

ABSTRACT

The occurrence of biofilms in drinking water distribution systems has caused more and more water quality problems and become a major concern to the industry. It is known that iron pipe materials support more biofilms than other materials, and the effect is positively related to the corrosion potential of the materials. It is also known that iron oxide tends to accumulate natural organic carbon on its surface. The purpose of this thesis is to investigate the hypothesis that the adsorbed humic substances on iron oxide surface can serve as carbon and energy sources for biofilm cells to grow.

To study the relationship between iron oxide, adsorbed humic substances, and biofilms, an iron oxide surface was created on glass beads and glass coupons by slow hydrolysis and condensation reactions of a millimolar solution of iron nitrate in approximately 10-mM nitric acid at 70 $^{\circ}$C. The physical, chemical, and mechanical properties of the surface were analyzed. The Elliot Silt Loam Soil humic substances were allowed to adsorb on the iron oxide surface in batch reactors. The adsorption isotherms at pH 6.7 and 7.4 were measured by TOC measurements. A desorption test was conducted to demonstrate the stability of the adsorbed humic substances. Four parallel plate flow cells with different coverslip surfaces were used for the biofilm growth studies. These coverslip surfaces included (1) glass, (2) iron oxide without pre-adsorbed humics, (3) iron oxide with pre-adsorbed humic of low surface coverage, and (4) iron oxide with pre-adsorbed humic of high surface coverage. A strain of *Pseudomonas aeruginosa* (PAO1, GFP+) was chemostat cultured and inoculated into the flow cells. It was allowed to attach and grow on the coverslip surfaces. These cells produced fluorescence and were counted by real time microscopy. A TOC free medium and a 0.25-ppm C humic substance medium were allowed to flow through the flow cells in a laminar mode. The biofilm densities and accumulation rates of the different surface and media conditions were measured and compared.

The results of this study demonstrated that (1) the iron deposit method provided a proper iron oxide surface for the subsequent humic adsorption and biofilm growth research. (2) The created iron oxide surface had significant adsorption capacity and affinity to the Elliot Silt Loam Soil humic substances. The adsorption could be interpreted by the modified Langmuir adsorption isotherm with multiple-layer adsorption. The adsorption decreased with higher pH. The desorption process of the adsorbed humic substances was very insignificant and neglectable. (3) Neither the iron oxide nor the adsorbed humic substances alone could support significant biofilm accumulation on the surface. However, the adsorbed humic substances could be an additional nutrient to assist higher accumulation rate of the biofilm on the surface. The adsorbed humic substances also helped to attract and maintain more bacterial cells on the surface.

CHAPTER 1. INTRODUCTION

With the increasing stringency in drinking water regulations over the past decades, concerns have been raised about biofilm growth in drinking water distribution systems and their impact on the health risk associated with tap water. A detailed study of biofilm growth is necessary to enable better control of it.

Drinking water is usually well treated and provides an unfavorable environment to bacterial growth: there is an extremely low level of nutrients and disinfectant is usually present. However, since biofilm cells grow on the water-solid interface of the pipe material surface, their physiological and ecological behaviors are different from planktonic bacteria. In addition, the chemical properties and nutrient conditions on the pipe material surface may be very different than that in the bulk water. Thus, to better understand biofilm growth, the following questions need to be answered:

- What are the chemical properties of the pipe material surface?
- Will the pipe material accumulate natural organic carbon at the water-solid interface?
- Will the chemical properties of the pipe material surface be changed after accumulating natural organic carbons?
- Is the accumulated natural organic carbon bioavailable?

Goals and Objectives

The main goal of this study is to provide working knowledge of the relationships between pipe materials and their corrosion products, natural organic carbon, and biofilm growth. Since ferrous pipes support more biofilm growth than other materials, and humic substances are the major organic carbon sources in the drinking water, this thesis will focus on the interaction among iron oxides, humic substances, and distribution biofilms.

Thesis Outline

The report of this study consists of four sections. Chapter 2 provides a comprehensive literature review of the research background and relevance. Chapter 3 describes the materials and methods used in this study to create a proper iron oxide surface, measure the adsorption of humic substances on the surface, and measure the biofilm growth on the surface. Chapter 4 reports the results of the research including the properties of the created iron oxide surface, the surface concentration of the adsorbed humic substances, and biofilm accumulation rate. These results were statistically compared for the different conditions. Chapter 5 presents the significance of the results of this study and compares them to the conclusions of other researchers. Chapter 6 presents a summary of the results and the primary conclusions drawn from this study.

CHAPTER 2. LITERATURE REVIEW

Bacterial Regrowth in Drinking Water Distribution Systems

Bacterial growth in drinking water systems has become a major concern due to degradation of water quality for the customers as well as industry. The growth of microorganisms in the distribution system may cause (1) increased hygienic safety and public health risks, (2) production of unpleasant taste and odor, (3) violation of the federal and state drinking water standards, and (4) high corrosion rate of pipe walls and pump casings.

Although drinking water is always fully treated and disinfected before leaving a water treatment plant, and the possible "breakthrough" of bacteria passing through the treatment and disinfection barrier (Camper, 1994) is minimized, the occurrence of coliform bacteria is still a widely spread problem in distribution systems (LeChevallier, 1990; LeChevallier et al., 1987; Herson, 1991). Experience has shown that maintenance of a chlorine residual can not be relied upon to totally prevent the occurrence of bacteria (LeChevallier et al., 1988). This chronic or periodic appearance of bacteria in the finished water has been termed "regrowth", and is presumed to be associated with the proliferation of bacteria within the distribution system (Camper, 1994).

In most drinking water distribution systems, the conditions for planktonic cell regrowth are unfavorable, considering the relatively short detention times, the low nutrient concentrations, and the presence of a residual disinfectant. In

contrast, conditions within water distribution systems can be favorable for attached biological growth. There is vast evidence showing that most pipe surfaces in distribution systems are colonized by biofilms. Research by van der Wende et al. (1989) and LeChevallier et al. (1990) shows that in a potable water distribution system, planktonic cell growth was negligible even in the absence of chlorine, and the coliform bacteria from distribution system biofilms had the same biochemical profile as organisms isolated from water column. It has been concluded that the significant increase of bacteria numbers in the drinking water distribution system is primarily due to the biofilms growing on the pipe walls, and detaching from the surface into the bulk water.

Biofilms in Drinking Water Distribution Systems

General

A biofilm is a layer of microorganisms in an aquatic environment held together in a polymeric matrix attached to a substratum (van der Wende and Characklis, 1990). Biofilms in distribution systems generally contain at least four components: water, microorganisms, extracellular polymeric substances (EPS), and organic or inorganic particles (Characklis and Marshall, 1990). Water provides a continuous liquid phase that fills a connected fraction of the biofilm volume and contains dissolved and suspended particulate materials. Biofilms from natural environments are generally heterogeneous, frequently containing more than one distinct microorganism. Both aerobic and anaerobic strata can be

found in the same biofilm. EPS are produced and excreted by microorganisms. The chemical structure and quantity of EPS production will vary among different types of bacteria and different environmental conditions (Abernathy, 1998). The organic and inorganic particles may be clay sediments or salt precipitation from bulk fluid, or the corrosion products from the pipe surface. These particles are adhered by the EPS.

Advantages to Bacterial Growth in Biofilm

The accumulation and development of biofilms provides a variety of ecological advantages to bacterial growth in flowing oligotrophic environment such as drinking water. The heterogeneous microenvironments in biofilm structure can be inhabited by bacteria of different physiologies (van der Wende and Characklis, 1990). The high flow rates of the water may transport tremendous amounts of nutrients to the fixed microorganisms. The solid-liquid interface (such as the pipe wall) and the EPS tend to adsorb natural organic matter from the water column, and may provide food for biofilm cell growth. The EPS anchor provides resistance to hydraulic and mechanical forces. The substratum surface and the EPS also protect bacteria from lethal levels of disinfectants due to possible chemical consumption of biocide and the transport limitations within the matrices (LeChevallier, 1990; van der Wende, Characklis and Smith, 1989).

Biofilm Formation

A biofilm is formed with the transport of microorganisms and nutrients to the substratum surface, followed by accumulation, growth, EPS formation, and detachment. The processes occurring during early colonization at the solid-liquid interface can be summarized as: substratum conditioning by organic molecules; transport of cells to the surface; initial reversible adhesion of cells to the substratum; desorption of reversibly adsorbed cells; transformation of reversibly adsorbed cells to irreversibly adsorbed cells; growth of irreversibly adsorbed cells; and erosion of cells from adsorbed colonies into bulk water (Mueller et al., 1992). The accumulation of biofilm cells results from the combination of attachment and reattachment, growth, and detachment.

Table 1. Some factors affecting biofilm growth in distribution systems.

Factors		Influences
Environmental Factors	Temperature	Higher temperature increases cell growth; Higher temperature increases nutrient level in raw water.
	Precipitation	Increases nutrient level in raw water.
Treatment Factors	Disinfectants	The cell killing performance varies with disinfectant types and dosages.
	pH	Physiologically affects cell growth; Affects the corrosion rate of pipe materials.
	Natural Organic Matters	The carbon and energy source for most heterogeneous bacteria. Can be controlled by various filtration methods.
Distribution Factors	Pipe Materials	Ferrous materials react with disinfectants, lower the residue level; The corrosion products benefit cell growth by providing more surface area, hiding from shear stress, and adsorbing nutrients.
	Hydraulic Regime	Influences the shear stress at the surface as well as the nutrients and disinfectants levels.

Factors that Influence Biofilm Growth

There are many factors related to microorganism growth in the distribution system (Camper, 1994; Martin et al., 1982). Some of the important factors and their influences are listed in Table 1. The actual effect on the presence of biofilms in the real world may be the combination of several or all of these factors. Among these factors, the pipe materials and the natural organic matter in the finished water are very important and considered in this study.

Pipe Materials and Their Effects on Biofilms in Distribution Systems

General

The nature of biofilms found in distribution systems is significantly affected by the materials of construction (Delanoue et al., 1997). A recent survey (LeChevallier et al., 1996) indicated that systems with more than 1,000 miles of unlined cast iron pipe had three-times-higher coliform levels than systems with 0 to 200 miles of unlined cast iron pipe. Experimental studies (Ollos et al., 1997) found that heterotrophic bacterial growth was 0.4 logs higher on ductile iron coupons than on polycarbonate substrata. A long-term study (Delanoue et al., 1997) showed that exposed iron supported more bacterial growth than cement, glass and other materials. Indirect evidence of reduction or control of bacterial regrowth by application of corrosion inhibitors (LeChevallier et al., 1990; Martin et al., 1982) also suggested the important relationship between ferrous materials and biofilm growth.

The advantage of iron pipe materials to biofilm growth has been attributed to the significant chlorine demand of iron and its corrosion products, which lower the disinfectant residual in finished water (LeChevallier et al., 1990, 1993; Chen et al., 1993). However, studies of an unchlorined system with 11% cast iron and 18% PVC (van der Kooij and Oorhuizen, 1997) showed that the biofilm density on cast iron pipe was two times higher than that on the PVC surfaces. The biofilm formation rate in the system was observed to increase with an increased iron accumulation due to the passage of water through cast iron pipes. Block (1992) concluded that under conditions of low or undetectable chlorine concentrations, there was a progressive decrease in bacterial densities on materials from cast iron, tinned iron, cement lined cast iron, to stainless steel. Camper et al. (1996) found that in the absence of a disinfectant, mild steel surfaces were consistently colonized by nearly 10-fold more heterotrophs and 2- to 10-fold more coliforms than were polycarbonate surfaces when the reactors were operated under the same conditions, and the impact extended to the effluent bacterial concentration as well. Studies (Camper, 1997; LeChevallier, 1997) also show that even with adequate corrosion control applied and consistent chlorine residues maintained, biofilm developed more quickly on iron pipe surfaces than on PVC pipes, and the iron pipe supported a more diverse microbial population than did PVC pipes in the studies. Therefore it can be concluded that iron materials in distribution systems not only protect biofilms from

the inactivity by disinfectants, but also enhance bacterial growth on their surfaces.

Unlined mild steel and unlined cast iron pipes comprise about 22% of all distribution pipes in the United States (LeChevallier, 1997). In many old cities where the distribution systems were built prior to 1940's, these materials may comprise of more than 80% of the distribution system (Abernathy, 1998). Therefore detailed studies of the physical and chemical properties of the materials and their corrosion products are very important to drinking water management.

Characteristics of Iron Pipe Materials

Unlined mild steel, followed by unlined cast iron and unlined ductile iron surfaces will support significantly higher biofilm density than PVC, cement, glass and other non-ferrous materials. This phenomenon can be explained by the high corrosion potential of the materials. Mild steel contains 99.12% iron by weight, while cast iron and ductile iron contain 93.18% and 92. 66% respectively. The exposed ferrous materials present 98.9% of the total area of mild steel and 83% and 81.5% for cast iron and ductile iron (Singley and Ahmadi, 1985). Increased exposed iron in the material leads to more release from the surface in the form of dissolved Fe^{2+}, and greater accumulation of corrosion products on the pipe surface. Iron corrosion products provide more surface area for bacteria colonization, protect cells from mechanical detachment, neutralize disinfectants,

and accumulate nutrients for biofilm growth (LeChevallier et al., 1996; Camper 1994; Martin et al., 1982; van der Kooij and Oorhuizen, 1997).

Corrosion of Iron Pipe Surfaces

In distribution systems, there are two ways for the corrosion of an iron pipe surface to occur. Chemically induced corrosion happens when an electrochemical potential difference exists between the pipe surface and the ions in the bulk fluid. This potential difference force electron transport from the pipe surface, resulting in the release of the more thermodynamically stable form of iron (Fe^{2+}). Microbiologically influenced corrosion (MIC) is caused by the chemical gradient developed between the pipe surface beneath a microbial colony and the bulk fluid. The chemical gradient creates an electrochemical cell that causes the pipe to release electrons and Fe^{2+} ions. Once released, Fe^{2+} reacts with various electron acceptors such as oxygen, free chlorine, and carbonate in the water to form corrosion products precipitated on pipe surface (Singley and Ahmadi, 1985).

Characteristics of Corrosion Product Surfaces

Goethite (α-FeOOH) and magnetite (Fe_3O_4) are the most common types of corrosion products found on iron pipe surfaces in distribution systems (Singley and Ahmadi, 1985). In aquatic environments, these iron oxide surfaces become "hydroxylated" through the sorption of a monolayer of water molecules. The hydroxylated sites behave much like diprotic acid, with the three potential species commonly represented as $\equiv FeOH^{2+}$, $\equiv FeOH$, and $\equiv FeO^-$ (Chang et al., 1997):

$$\equiv FeOH^{2+} \leftrightarrow \equiv FeOH + H^{+} \qquad pKa1 \qquad (1)$$

$$\equiv FeOH \leftrightarrow \equiv FeO^{-} + H^{+} \qquad pKa2 \qquad (2)$$

At least two types of surface hydroxyl groups have been identified on iron oxides (Parfitt et al., 1977). The OH groups that bind to two Fe ions are more strongly polarized, more acidic, and relatively less intractable with anions. The single-bounded OH groups, on the other hand, are less polarized, and more basic in nature. They are possibly exchangeable with other anions in solution, such as phosphate and sulfate. They may also be exchanged with the hydroxyl or carboxyl groups of natural organic matter (NOM), resulting in the accumulation of NOM onto the iron oxide surface.

The adsorption of NOM may be the most important surface property of iron oxide in drinking water distribution systems and treatment. Iron oxides may be used as a filter medium to remove NOM from the finished water (Benjamin et al., 1993; Benjamin and Li, 1997), lower the nutrient level, and subsequently lower the bacteria regrowth potential. In distribution systems, iron oxides, as the most common corrosion products on pipe surface, are capable of adsorbing organics from the bulk water, and may provide a higher concentration of organic carbon on the pipe surface than in the bulk fluid (van der Wende and Characklis, 1990). The adsorption to the iron oxide surface may also increase the bioavailability of the carbon substrates for microorganisms. Thus, the higher occurrence of biofilms on iron pipe materials may be partially a result of the adsorption of NOM on the iron oxide surfaces.

Natural Organic Matters and Their Effects on Biofilms in Distribution Systems

General

Carbon, nitrogen, and phosphorous are the principle nutrients for the growth of heterotrophs and coliform bacteria. Other factors such as trace metals and organic cofactors may also be necessary for bacterial growth, but they are usually presumed to be non-limiting in a mixed microbial population (Camper, 1994). Organic carbon is utilized by bacteria to produce new cellular materials and provide energy, while nitrogen and phosphorous are required for biosynthesis. Because the growth of heterotrophic bacteria generally requires carbon, nitrogen, and phosphorous in a ratio of approximately 100:10:1, organic carbon is the growth-limiting nutrient (LeChevallier, 1990), and an important factor for understanding biofilms in distribution systems.

Sources of Natural Organic Matter

Natural organic matter (NOM) in surface waters come from a variety of sources. The biodegradation of plant and animal remains by microorganisms produces large amounts of organic materials in soil. These organic materials can be washed into the freshwater environment. Biodegradation and leaching of organic detritus from soil in the watershed are the major source of NOM in natural water environment (Aiken and Cotsaris, 1995). Microbial degradation of plants in lake and river systems releases NOM directly into water.

Photosynthesis by phytoplankton also provides a small portion of NOM (Wetzel, 1992).

The source of NOM significantly impacts its chemical composition. Freshwater environments content more high molecular weight (HMW) compounds, such as humic substances, than low molecular weight (LMW) compounds. In marine systems the LMW compounds, such as amino acids and carbohydrates, are dominant (Amon and Benner, 1996). Water sources from areas with wetlands and forests may have a high amount of humic substances, while water sources from agricultural areas may have more nitrogen-containing organics (Aiken and Cotsaris, 1995).

Measurement of Natural Organic Matter

In drinking water distribution systems, the amount of NOM in finished water is traditionally measured by total organic carbon (TOC) or dissolved organic carbon (DOC). In the USEPA's National Organic Reconnaissance Survey (Symons et al., 1975), the non-purgable TOC concentration of finished water in 80 locations ranged from 0.05 to 12.2 mg/L. The TOC level in drinking water is impacted by several factors, such as seasonal temperature and rainfall. LeChevallier et al. (1991) found that coliform bacteria always occurred in the distribution system when TOC levels were greater than 2.9 mg/L, while TOC levels below 2.2 mg/L were associated with very low coliform levels. However, other researchers (van der Kooij et al., 1982) have indicated that measurement

of TOC was unreliable for predicting microbial growth, because only a small portion of the TOC pool is normally available for biodegradation.

Several techniques have been developed to measure the biodegradable portion of TOC or the biological stability of drinking water. These techniques include biodegradable organic carbon (BDOC) and assimilable organic carbon (AOC). BDOC is the portion of organic carbon in water that can be mineralized by heterotrophic microorganisms (Huck, 1990), and can be determined by measuring the change in TOC after the water passing through a packed bed bioreactor (Lucena et al., 1990). Servais et al. (1991) have estimated that biological stability can be achieved when BDOC levels were less than 0.2 mg/L. AOC is the portion of biodegradable organic carbon that can be converted to cell mass and expressed as a carbon concentration by means of a conversion factor or calibration (Huck, 1990). AOC is measured by a batch culture of *Pseudomonas fluorecens* (P17 strain) and *Spirollum* (NOX strain) (van der Kooij et al., 1982). Van der Kooij (1992) found that AOC levels greater than 10 μg C/L would support heterotrophic plate count growth in distribution system. LeChevallier et al. (1990) determined a threshold AOC level of 50 μg C/L for heterotrophic growth.

Types of Natural Organic Matter

The type of NOM in distribution system also influences the AOC or BDOC level, and the growth of microorganisms. Figure 1. illustrates the available NOM for microbial growth in drinking water (Kaplan et al., 1994). The sources of this

NOM can be characterized as humic and non-humic substances. Non-humic substances are those materials that can be placed in one of the categories of discrete compounds such as carbohydrates, amino acids, fats and so on. Humic substances are the other unidentifiable compounds with relatively high molecular weight. Humic substances and humic-bound organics comprise the majority of NOM in finished water.

Sources of Humic Substances

Humic substances are naturally occurring organic materials that result from random condensation of the microbial decomposition products of living organisms (mostly plants) and their residues. They largely exist in soil as well as the water environment, and play important functions in nature such as increasing buffering and exchange capacity of soils. Several pathways exist for the formation of humic substances during the decay of plant and animal remains (Stevenson, 1982). Each involves different intermediates, such as lignins, polyphenols, quinones, simple sugars and amino compounds. The chemical structure of humic substances is dependent on its source. Lignin-derived substances tend to be more aromatic, having more benzene- and phenol-like components, and are low in nitrogen content. Microbially derived substances are more aliphatic and high in nitrogen content (Aiken and Cotsaris, 1995). In practice all the pathways must be considered as likely mechanisms for the synthesis of humic substances. Therefore humic substances, rather than

being pure chemicals, are heterogeneous mixtures of complex materials containing aromatic and aliphatic fractions.

Types of Humic Substances

In the laboratory, humic substances can be separated from soil by application of alkali, gel chromatography, ultrafiltration, and ion-exchange methods. Humic substances can be divided into three categories: fulvic acid, humic acid, and humin. Fulvic acid is the fraction that is soluble in water under all pH conditions. It has the lowest degree of polymerization, with a molecular weight as low as a few hundreds. Fulvic acids have the lowest carbon content but the highest oxygen content and exchange acidity. Humic acid is the fraction that is not soluble in water under acidic conditions (pH < 2) but is soluble at higher pH values. Its molecular weight is in the several thousands range demonstrating a higher degree of polymerization. It has higher carbon content than fulvic acid but lower oxygen content and exchange acidity. Humin is the fraction that is not soluble in water at any pH value. It has the highest molecular weight and carbon content but lowest oxygen content and acidity (Stevenson, 1982). Humic and fulvic acid are the major humic substances in aquatic environments due to their solubility. The typical molecular weights for aquatic humic acid and fulvic acid are 3,000 and 500-1,000 respectively (Malcolm, 1985). Humic acids are the major extractable component of soil samples, while typically 90% of dissolved humic substances in natural water are fulvic acids and the remaining 10% are humic acids (Beckett, 1990; Benjamin et al., 1993).

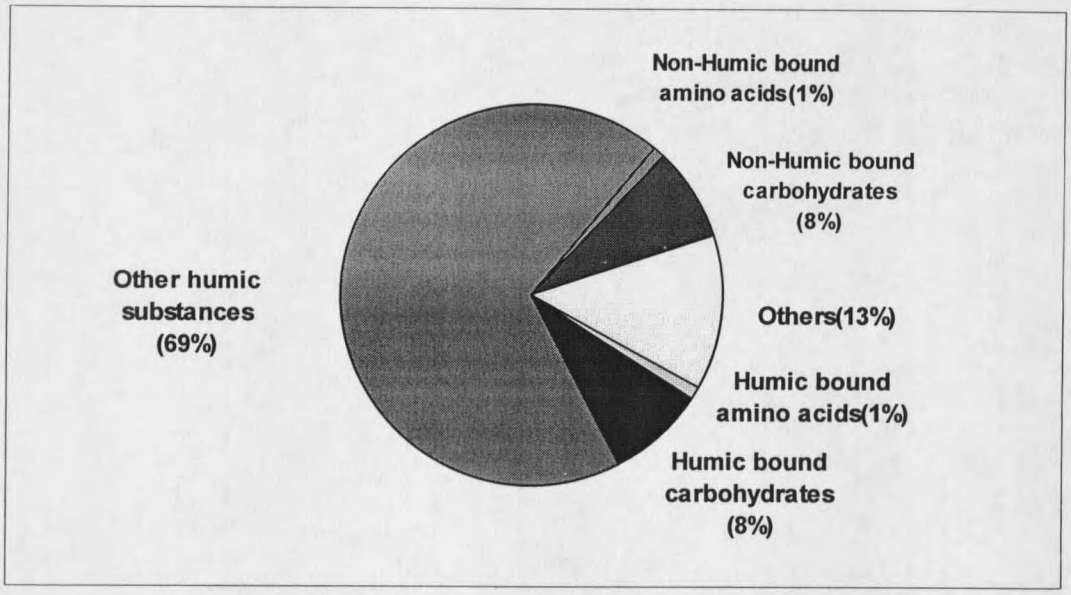

Figure 1. Type of natural organic matter in surface water. (Kaplan et al., 1994)

Structures of Humic Substances

It is apparent that humic substances consist of a heterogeneous mixture of compounds for which no single structural formula will suffice. Model formulas of humic and fulvic acid in Figure 2 may hypothetically illustrate the structures of the acids (Stevenson, 1982). Humic acids are thought to be complex aromatic macromolecules with amino acids, amino sugars, peptides, and aliphatic compounds involved in linkages between the aromatic groups. The model structure contains free and bound phenolic OH groups, quinone structures, nitrogen and oxygen as bridge units and COOH groups at various places on aromatic rings. The model structure of fulvic acid contains aromatic as well as aliphatic structures, both extensively substituted with oxygen-containing functional groups.

There is a greater aromatic portion in humic acid than in fulvic acid, which accounts for the higher carbon content in humic acid. Fulvic acids contains more functional groups of an acidic nature, particularly COOH, resulting in higher acidity (900-1400 meq/100g) than humic acid (400-870 meq/100g). Another important difference is that while the oxygen in fulvic acid can be accounted for largely in known functional groups (COOH, OH, C=O), a high portion of the oxygen in humic acid seems to occur as a structural component of the nucleus (Stevenson, 1982).

Although aquatic humic acids and fulvic acids vary in composition, their similarities are more pronounced than their differences (Malcolm, 1986). Carbon,

hydrogen, oxygen, and nitrogen are the major chemical components for all of them. Both acids contain carboxyl, phenolic hydroxyl, and alcoholic hydroxyl groups as their major functional groups. Under the neutral pH conditions of fresh waters, many functional groups are ionized and negatively charged. The anionic charge accounts for many properties of humic substances, including their aqueous solubility, buffer capacity, and binding capacity for metals. Humic substances can form stable complexes with metal ions, especially the transition elements (Weber, 1988). The complexation ability may even increase if the carboxyl groups are in favorable steric arrangements to chelate with metal ions (Chang, 1992). Humic substances also tend to accumulate on metal oxide surfaces, which will be discussed in the following section.

Bioavailability of Humic Substances

In the bulk fluid, humic substances are found in a tightly coiled conformation (Chang, 1992). Electron microscope observations also show colloid structures of humic acids in the natural environment (Weber, 1997). The coiled structures may decrease the bioavailability of humic substances to suspended bacteria because the enzymatically active site of the molecule may be hidden deeply in the colloid, unreachable by microorganisms. It was found that humic substances could form complexes with extracellular enzymes, inhibiting the action of those enzymes. Divalent cations, such as Ca^{2+} and Mg^{2+}, can prevent the formation of humic-enzyme complexes; it has been found that bacterial productivity on humic substances in hard water was greater than in soft water

(Welzel, 1992). Billén (1991) also indicated that polymeric substances were partially recalcitrant to degradation and their assimilation requires extracellular hydrolysis. This evidence implies that microorganisms cannot effectively utilize the dissolved humic substances as nutrient sources. In practice, humic substances in natural water environments are very stable and resistant to microbial degradation (McKnight, 1990). However, Lovley et al. (1996) found that some microorganisms in soils and sediments were able to use humic substances as electron acceptors for the anaerobic oxidation of organic compounds and hydrogen. Other researchers (Sunda and Kieber, 1994; Stone, 1987) reported that Mn oxides could degrade humic substances to form low molecular weight organic compounds that could be used as substrates for the growth of some Mn-oxidizing bacteria. Thus, the biological properties of humic substances are still under investigation.

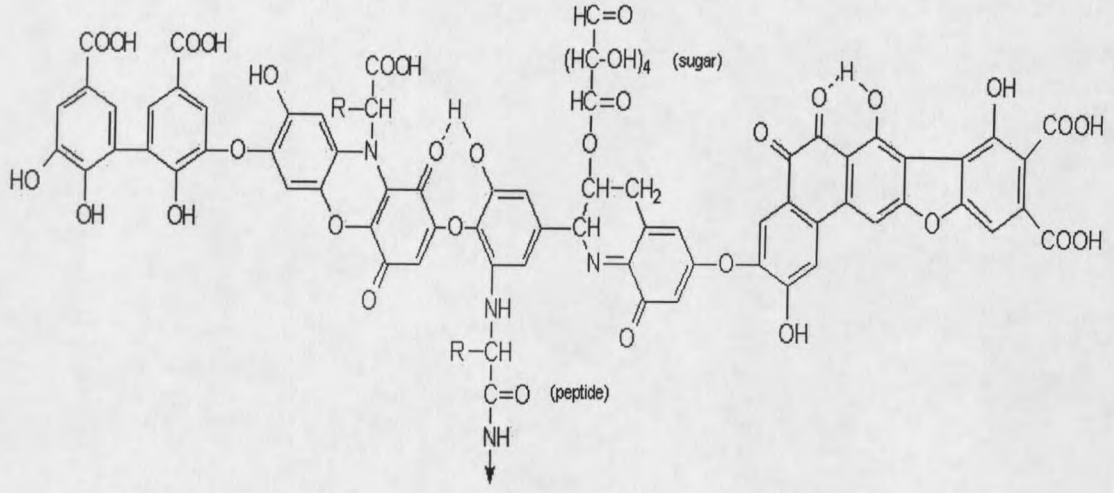

Humic Acid

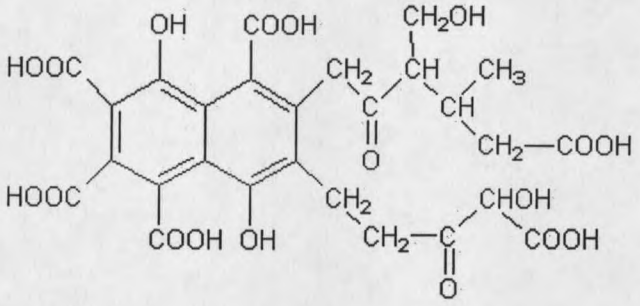

Fulvic Acid

Figure 2. Model structures of humic acid and fulvic acid. (Stevenson, 1982)

Adsorption of Humic Substances on Iron Oxide Surfaces

General

Aquatic humic substances strongly adsorb to iron oxide surfaces in natural environments (Tipping et al., 1981) as well as under laboratory conditions (Gu et al., 1994; Tipping, 1980; Parfitt et al., 1977; Varadachari et al., 1997). This process can mask the physicochemical properties of the underlying iron oxide whose surface behavior may become dominated by the adsorbed organic matter. The adsorption may also influence the chemical and biological properties of humic substances.

Mechanisms

The mechanisms by which humic substances adsorb onto mineral surfaces include anion exchange (electrostatic interaction), ligand exchange-surface complexation, hydrophobic interaction, thermodynamic effect, H-binding, and cation bridging (Gu et al., 1994). Infrared spectroscopy (Parfitt et al., 1977) and adsorption heat measurements (Gu et al., 1994) suggested that ligand exchange is the most important mechanism for the adsorption of humic substances to iron oxide surfaces. The mechanism is shown in Figure 3. The hydroxylated oxide surface, behaving as a Lewis acid, can exchange OH^- ion against the anionic group of humic acid and fulvic acid. This process occurs when the anionic group penetrates the coordination shell of Fe and displaces the OH^- by COO^-. At low surface coverage, humic matter may be adsorbed to the surface by multiple binding groups on each molecule, and each binding group

may coordinate with more than one surface site. As more molecules adsorb, it becomes less likely that one binding group will associate with more than one surface site. As the surface becomes even more crowded, few or only one binding group may participate in the coordination, and the rest of molecule may extend into the bulk fluid to minimize the repulsive forces between charged groups on individual or adjacent molecules (Tipping, 1981).

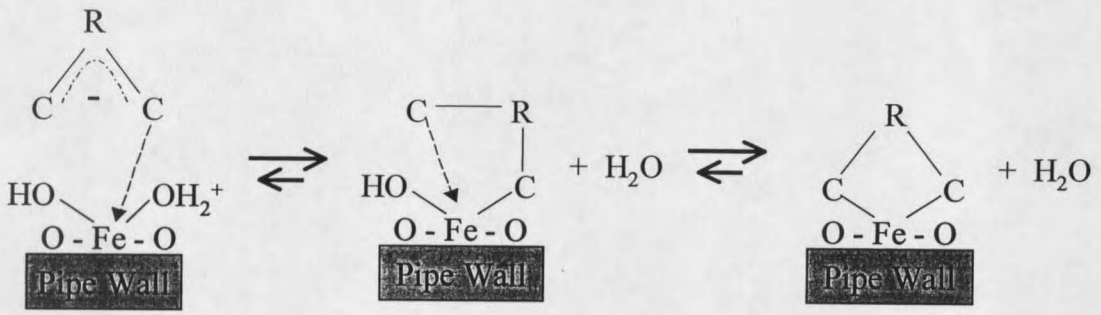

Figure 3. Schematic of ligand exchange adsorption of humic substances onto iron oxide surfaces.

Mathematical Models

Considering the heterogeneity of substratum surfaces as well as humic substances, and the possibility that both chemical and physical adsorption may occur at the same time, it is very difficult to make a concise description of the adsorption of humic substances at a water/solid interface. However, several empirical models have been still developed to mathematically describe the phenomenon (Tipping, 1981; Gu et al., 1994; Chang, 1992). The Langmuir isotherm was commonly used to interpret reactions between macromolecular solutes and solid surface at the interface (Adamson and Gast, 1997). Originally developed to describe the adsorption of a gas on solid surfaces, the Langmuir model assumes that only a monolayer of adsorbate molecules accumulates on substratum surface, and the already adsorbed molecules have no impact on further adsorption. However, for the adsorption of humic substances on iron oxide surfaces, these assumptions may not be true. Considering the large molecular size and the negative charge, humic molecules may interact with each other during the adsorption, resulting in changing adsorption energy. The adsorbed humic molecules may also catch other molecules to form multiple layer adsorption. Tipping (1981) has reported non-Langmuir adsorption and attributed it to an approximately doubled adsorption capacity for humic substances.

The Langmuir adsorption model also assumes constant adsorption energy throughout the overall process. But in the real world, the adsorption energy may be related to the surface coverage because the previously adsorbed humic

molecules may influence subsequent adsorption by electrostatic or thermodynamic effects (Gu et al., 1994). The energy of the multiple layer adsorption which occurs between humic molecules is also not same as that for the monolayer adsorption which occurs between humics and iron oxides. Thus, a modified Langmuir model was developed by Gu et al. (1994) to take the adsorption energy change into account. By changing the values of the coefficients, this model is capable of fitting a variety of adsorption isotherms including L-type, S-type, H-type, and C-type isotherm (Gu et al., 1994).

The modified Langmuir model considers the adsorption process to be reversible as described in equation 3, where C is the solution humic concentration, S is the available surface sites on the adsorbent for humic adsorption, and q is the surface concentration of the adsorbed humics. S is equal to ($q_{max} - q$), where q_{max} is the maximum quantity of humic substances that can be adsorbed.

$$C + S \underset{k_b}{\overset{k_f}{\Leftrightarrow}} q \qquad (3)$$

The parameters k_f and k_b are the forward and backward rate coefficients with corresponding to the activation energies of adsorption (E_f) and desorption (E_b):

$$k_f = Ae^{(-E_f/RT)} \qquad (4)$$

$$k_b = Be^{(-E_b/RT)} \qquad (5)$$

where A and B are the frequency factors, R is the universal gas constant, and T is the absolute temperature.

The activation energies E_f and E_b are used to account for the heterogeneity of adsorbent surfaces and adsorbates, which ultimately influence the adsorption affinity of humic substances. Showed in equation 6 and 7, These two parameters are linearly related to the surface coverage, where E_f^0 and E_b^0 are the energies of adsorption and desorption at q = 0, and θ is the surface stress coefficient.

$$E_f = E_f^0 + \theta q \tag{6}$$

$$E_b = E_b^0 + \theta q \tag{7}$$

The net rate of adsorption can be expressed as:

$$\partial q/\partial t = k_f C(q_{\max} - q) - k_b q \tag{8}$$

Substitution of equations 4, 5, 6, and 7 into equation 8:

$$\partial q/\partial t = Ae^{(-E_f^0/RT)} C(q_{\max} - q)e^{(-\theta q/RT)} - Be^{(-E_b^0/RT)} q\, e^{(\theta q/RT)} \tag{9}$$

For equilibrium adsorption, $\partial q/\partial t = 0$. By defining

$$K = (A/B)e^{-(E_f^0 - E_b^0)/RT} \tag{10}$$

$$b = \theta/RT \tag{11}$$

Equation 9 can be rearranged to equation 12 and 13 as the general form of the model:

$$q = \frac{K_q q_{\max} C}{K_q C + 1} \tag{12}$$

where

$$K_q = K e^{-2bq} \tag{13}$$

Constant q_{max}. q_{max} is called the adsorption capacity indicating the maximum amount of humic substances that can be adsorbed on the iron oxide surface. No more humics are able to accumulate even if the solution concentration goes higher. The presence of q_{max} for a given water/solid system was widely reported (Tipping, 1981; Gu et al., 1994; Parfitt et al., 1977; Kummert and Stumm, 1980), and is an essential assumption of the model. q_{max} represents the surface property of the substratum, i.e., the adsorption site density. As previously mentioned, in aqueous systems iron oxide surfaces are hydroxylated in terms of $\equiv FeOH^{2+}$, $\equiv FeOH$, and $\equiv FeO^-$ (Chang et al., 1997). The chemical adsorption of humic substances on these surfaces involves a ligand exchange reaction, in which the carboxyl functional groups of humic molecules bind directly with the Fe ions by replacing the reactive surface hydroxyl groups. Thus, each exposed Fe ion becomes a center for the adsorption. The more Fe ion on the surface, the higher the q_{max} value.

Constant K. K is called the adsorption affinity, indicating the potential that humic molecules will accumulate on the iron oxide surfaces. At very low free

humic concentration in bulk solution (i.e., $C \rightarrow 0$ and $q \rightarrow 0$), equation 12 can be simplified to equation 14:

$$q = Kq_{max}C \qquad (14)$$

Thus, both q_{max} and K contribute to the initial adsorption rate of the system, where q_{max} tells how many sites are available, and K tells how likely the process will occur.

Constant b. If the adsorption affinity remains constant throughout the whole adsorption process, equation 12 becomes the Langmuir model. This kind of adsorption was observed by several researchers (Tipping, 1981; Gu et al., 1996). However, some non-Langmuir adsorption was also reported (Tipping, 1981; Gu et al., 1994). As mentioned above, both iron oxide surfaces and humic substances present great heterogeneity. Different chemical adsorption procedures as well as physical adsorption may occur in the same system. Thus, a constant adsorption affinity is certainly dubious in many systems. In the modified Langmuir model, the surface excess-dependent affinity K_q was defined as a function of q, and the constant b was used to take into account the features of changing energies of adsorption with changing surface coverage. When b = 0, which represents a constant energy of adsorption, K_q = K, and equation 13 becomes Langmuir isotherm.

Desorption

As described in equation 3, the ligand exchange reaction is usually considered reversible, and mathematical models of transport often predict that

desorption reactions occur in the same way as adsorption. However, researchers (Gu et al., 1994) have found that humic substances, once adsorbed, are very difficult to desorb at a given pH and ionic composition. Although irreversible adsorption is thermodynamically impossible, the kinetics of desorption may be unobservablly slow comparing to adsorption, resulting in a hysteresis of the adsorption-desorption reaction.

Factors Influencing the Adsorption of Humic Substances onto Iron Oxides

The adsorption capacity of humic substances onto iron oxide surfaces depends on a variety of factors, including the type of humic substances, type of iron oxides, pH value of the bulk fluid, and presence of cations as well as anions (Davis and Gloor, 1981; Gu et al., 1996; Tipping, 1981; Parfitt, 1977; Davis, 1982; Varadachari et al., 1997). The combination of the impacts of these factors makes adsorption very complicated, and only a limited understanding of the phenomenon exists. Only empirical explanations exist for the phenomenon.

Types of Substance. Aquatic humic and fulvic substances are mixtures of organic compounds with different molecular sizes and different compositions. Davis and Gloor (1981) have found that the percentage of DOC adsorbed on oxides increased with increasing molecular weight (MW) of the humics; 65% for the fraction with MW > 4,000, 40% for 500 < MW < 4,000, and 20% for MW < 500. They also indicated that organic compounds with MW greater than 1,000 formed strong complexes with the oxide surfaces, but low MW compounds were weakly adsorbed, unless the compounds contained functional groups that could

specifically coordinate with the oxide surface. Most of the adsorbed organic compounds were in the MW range of 1,000 to 3,000. Data from Varadachari et al. (1997) show higher adsorption capacity of humic acids than fulvic acids by goethite and hematite at various pH values. Larger humic compounds contain more functional groups, and may tend to coordinate with more oxide surface sites at the same time than smaller molecules, leading to stronger overall binding force (Davis, 1982). Thus the adsorption affinity of large organic molecules is higher than that of smaller ones.

Gu et al. (1996) indicated that different organic compounds or fractions of humic substances show different adsorption affinities and capacities on iron oxide surfaces. Compounds or their subcomponents with higher carboxyl functional group density and extended molecular structure presented stronger surface complexation with iron oxide, resulting in higher adsorption potential. When the surface sites were limited, these compounds or their subcomponents competed with each other for adsorption.

Types of Iron Oxide. Different types of iron oxide have different Fe:O ratios, different crystal style, and subsequently different surface areas and exposed iron content at the oxide surface. Thus their adsorption potentials with humic substances are not the same. Tipping (1981) reported that goethite had higher humic acid adsorption capacity (the maximum amount of humics that could be adsorbed) but lower adsorption affinity (the available amount of adsorption sites) than hematite at a pH of about 7. However, other researchers

(Varadachari et al., 1997) reported higher fixation of humic acid by hematite than by goethite at all pH values greater than 7.0. The disagreement between these reports may be due to the complexity of the materials, their oxide sources and experimental methods. Varadachari et al. (1997) also indicated that the higher adsorption capacity of hematite might be attributed to its strong potential for cation-bridging adsorption.

pH. The adsorption of humic substances on iron oxide is strongly pH-dependent. Tipping (1981) found that the extent of adsorption of humic acids on goethite decreased with an increase of pH. Similar trends were also reported by other researchers (Gu et al., 1994; Parfitt, 1977; Davis, 1982). This effect is attributed to the deprotonation of the hydroxylated oxide surface. Shown in Equations (1) and (2), when the pH of the bulk fluid increases, the balances will shift to the left, and change $FeOH^{2+}$ and FeOH to FeO^{-}. As O^{-} ion is a stronger Lewis base than OH^{2+} and OH, it is less exchangable by the carboxyl group on humic molecules, resulting in a decrease of available adsorption sites and subsequently a lower adsorption capacity. The deprotonation of iron oxide surface sites as well as the carboxyl groups of humic substances may also enhance the electrostatic repulsion between them and reduce the adsorption affinity, although this effect is not as significant as the surface site reduction (Gu et al., 1994; Tipping, 1981).

Presence of Cations. As described in the previous section, carboxyl and hydroxyl functional groups of humic and fulvic acids are known to form very

stable complexes with many metal cations or hydroxylated metal cations. Thus the presence of metal cations in the bulk fluid will impact the adsorption of humic substances to iron oxides. Varadachari et al. (1997) reported that the existence of di- and trivalent ions increased the fixation of humic acids on goethite, while monovalent ions decreased the fixation. They explained the effects by a cation-bridging adsorption mechanism of binding the negatively charged humic molecule and iron oxide surface through the positively charged cation. Tipping (1981) also reported an increase of humics adsorption capacity on goethite with the presence of Ca^{2+} and Mg^{2+}. He explained the effect by the competition of cations with the oxide for anionic groups on the humics. The humics could then have fewer contacts per molecule with the oxide surface, resulting in the adsorption of more humic molecules at a lower affinity. Gu et al. (1994) reported that monovalent ions such as Na^{+} had no effect on humics adsorption. The existence of cations also neutralizes the negative charge of anionic groups of humics, reducing the electrostatic repulsion that prevents the adsorption (Chang, 1992).

Presence of Inorganic Anions. Gu et al. (1994) estimated that phosphate and sulfate anions substantially reduced humic substance adsorption on iron oxide surfaces. The effect of phosphate was greater than sulfate. These effects were due to the specific adsorption of these anions on the oxide surface.

Influences of Adsorption of Humic Substances to Iron Oxide surfaces

Humic substances are some of the most powerful metal-binding agents found in natural organic matter. The adsorption process includes a variety of physical and chemical interactions between iron oxides and humics. Consequently these interactions will influence the physical, chemical, and even biological properties of both iron oxide surfaces and humic substances.

Impact to Iron Oxide Surface. The adsorption of humic substances can mask the properties of the underlying iron oxide and present a surface with very different physicochemical behaviors. Electrophoresis studies have demonstrated that iron oxide surfaces become negatively charged after adsorbing natural organic materials (Davis and Gloor, 1981; Tipping and Cooke, 1982; Beckett, 1990). Tipping (1982) indicated that the large molecular size of humics caused the plane of electrokinetic shear to be at some distance from oxide surface, positioned at or near the outer parts of the humic molecules. The shear potential was therefore due to the ionized (anionic) humic functional groups not involved in adsorption with the oxide surface. The negative potential increased significantly with the increase of adsorption density at low free humic concentrations. At high free humic concentrations, however, protonation of the unadsorbed humic groups increased as a result of the accumulation of protons in the diffusion double layer in response to the negatively charged fixed layer and the lower dielectric strength of the fixed layer compared to the bulk solution. The increasing negative charge effect by additional adsorption was reduced. The presence of calcium and

magnesium ions will also significantly reduce the negative charge on the adsorbed humic substance surfaces. At humic concentrations greater than about 1 mg/L, differences in Ca^{2+} concentration can affect the magnitude of the charge just as much as differences in humic concentration (Tipping, 1982). Ca^{2+} and Mg^{2+} behave analogously to protons, but bring more positive charge to the shear plane, making the surface less negative. Ca^{2+} interacts more strongly with the COO^- groups of the adsorbed humics than does Mg^{2+}. Results from Tipping (1982) also show that Na^+, at high concentration (greater than 0.04 M) reduced the negative charge, but with a much less impact.

Impact to Humic Substances. In aquatic environments, humic substances tend to form coiled structures (Chang, 1992; Weber, 1996), with the more hydrophilic carboxyl and hydroxyl groups spreading outside, and the more hydrophobic portions, such as peptides, lipids and polysaccharides wrapped inside. After the adsorption to iron oxide surfaces, humic substances are likely to collapse on the surfaces to allow for maximum points of interaction between their O-containing functional groups and iron oxide surfaces through either ligand exchange or H-bonding mechanisms (Gu et al., 1994; Davis, 1982). This collapse may force the humic molecules to be uncoiled, increasing the bioavailability of the previously hidden sites.

Summary

Aquatic humic substances, including humic acids and fulvic acids, are naturally abundant organic matter in freshwater as well as in drinking water distribution systems. They have very strong potential to adsorb onto iron oxide surfaces, which are the major corrosion products of the widely used iron pipe material in distribution systems. In oligotrophic environments, such as distribution systems, this adsorption process will fix and concentrate the trace amount of humic substances on the pipe surface. The bioavailability of humic materials may also increase due to the adsorption. Microorganisms may then utilize these adsorbed humics as carbon and energy sources to form biofilms, and degrade the quality of finished water by releasing cells into water. Thus, in order to better understand of the nature of biofilm regrowth, and to effectively control the problem, it is necessary to study the relationship between adsorbed humic substances on iron oxide surfaces and the growth of biofilms.

CHAPTER 3. MATERIALS AND METHODS

Introduction

The purpose of this research was to estimate bacterial growth potential on humic acids, which were adsorbed on iron oxide surfaces. To do so, we have (1) created a α-FeOOH (goethite) surface on both glass bead and glass coverslips; (2) measured the adsorption capacity of this surface to Elliot Silt Loam Soil humic acid; and (3) examined the attachment and growth behavior of *Pseudomonas aeruginosa* on the surface with humic acid as the only carbon source.

Creation of Iron Oxide Surface

General

A proper iron oxide surface was needed to achieve our goals of humics adsorption and biofilm growth potential measurements. This surface should have significant surface area and adsorption capacity to humic substances; it should be stable in aqueous solution; it should be transparent allowing the observation of bacterial accumulation; it should be uniform and easy to make. A thin goethite ($^{\alpha}$-FeOOH) film on glass supporting materials was the choice because goethite is the most common iron oxide in water distribution systems and it has a higher adsorption capacity for humic substances than other iron oxide materials (Abernathy, 1998). Glass was used as it was available in both micro beads and coverslips. Micro glass beads had significant specific surface area for the

adsorption measurement, and the coverslip worked for microscopic observation of attached bacterial growth.

Various techniques have been developed to coat iron oxides on solid supporting materials. Chang (1992) and Benjamin et al. (1997) coated sand and olivine by wrapping them with an iron oxide sludge made from ferric chloride and sodium hydroxide, and heating them to 110 °C. This coating was mainly hematite, and unstable in water solution (redissolved). The coating was also totally untransparent, limiting its use for microscopic observation needed for this study. Rieke et al. (1994, 1996) reported the formation of thin goethite films on a silicon substratum by thermal hydrolysis of millimolar aqueous solution of $Fe(NO_3)_3$ at a pH of approximately 2.0. In our study, a simplified procedure with multiple coating was used to create a thicker layer of goethite on the glass substratum.

Glass Beads

Micro glass beads (size #130, Rascher & Betzold) were used as the supporting material for the adsorption experiments. The beads had a density of 2.46 to 2.49 g/cm^3. Micrometer measurement showed that the diameters of the beads were in the 110 to 130 μm range. The beads were sonicated in chloroform (HPLC grade, Fisher Scientific) for 30 minutes, in 0.22-μm filtered 0.1 M KOH for 10 minutes, and in 0.22-μm filtered 0.1 M HNO_3 for 10 minutes to remove any adsorbed organic and inorganic matter. The beads were then rinsed in 0.22-μm

filtered nanopure water until the pH of the water reached neutrality. Finally the beads were dried at 110 °C for 20 hours, and stored in a glass bottle.

Glass Coverslip

The glass coverslip (Eric Scientific) used in the growth experiments had a size of 43 mm x 61 mm, and thickness of 40 ±10 μm. It was sonicated in chloroform for 30 minutes, then acid-cleaned in a bath of NoCromix (Cleaning solution with concentrated H_2SO_4, Godax Laboratories) for 12 hours. After being rinsed in 0.22-μm filtered nanopure water, the coverslip was wrapped in foil and baked in a 300 °C oven for at least 8 hours. The cleaned coverslip was stored in a sealed glass petri dish.

Coating Solution

A freshly made coating solution with 3 mM $Fe(NO_3)_3$ and 10 mM HNO_3 was prepared by dissolving 1.212 g hydrated ferric nitrate ($Fe(NO_3)_3.9H_2O$, recently ordered, Mallinckrodt Baker) into 1 liter of 10 mM HNO_3 (diluted from 1 M HNO_3 which was titrated by 1 M NaOH). The solution was rapidly stirred, filtered with a 0.22-μm membrane filter, and used immediately. The solution had a slight yellow color with a pH of about 2.1.

Iron Oxide Coating Process

A schematic of the coating process is shown in Figure 4. A column (14-inch long, 7/8-inch inner diameter) was made by Teflon tubing (FEP, McMaster Carr) with stainless steel fittings and 100 mesh sieves on both ends. A polypropylene isolation material was wrapped outside of the column to maintain

the temperature. About 100 g of cleaned beads were freely packed into the column and filled two thirds of the volume. A 250-ml bottle (FEP with ETFE closure, Nalgene) holding 200 ml coating solution was connected to the column with tubing (PharMed, Cole-Parmer). By using a peristaltic pump (Cole-Parmer), the solution was recycled between the bottle and the column at a rate of 160 ml/min to form a stable bed in the column. The solution bottle was held in a water bath, and the temperature was increased slowly from ambient temperature to 85 °C, allowing the temperature in the column to reach 70 °C. The solution changed from light yellow to light brown in color after about three hours running, and was then replaced with fresh solution. A total of three bottles of solution were used for the entire coating process, and the beads were finally coated with a dark orange color iron oxide. After cooling down, the beads were unpacked into a large flask, and rinsed with 0.22-μm filtered nanopure water several times until no significant color appeared in the water. The beads were then repacked into the column, and dried with nitrogen gas. The nitrogen also protected the coating from further oxidation by air. The dry beads were stored in a glass bottle.

A similar coating procedure was used for the glass coverslip. The cleaned coverslip was held in a pre-cleaned glass jar with 200 ml coating solution. The jar was submerged in a water bath, and the temperature was allowed to increase slowly from ambient temperature to 70 °C. The solution changed to a light brown color after about two hours, and was then replaced. In total, three bottles of solution were used for the entire coating process, and the coverslip was finally

coated with a dark orange, shining, transparent iron oxide film. It was rinsed in 0.22-μm filtered nanopure water and blown dry with nitrogen gas. The coated coverslip was stored in a sealed petri dish.

Characteriztion of the Iron Oxide Surface

Digestion Test - Mass of the Iron Oxide Film

The mass of the iron oxide film was determined by acid digestion of the iron oxide. Twenty g of the coated beads were weighed accurately in a 250-ml flask that had been acid cleaned and baked at 300 °C for eight hours. 100 ml of a 10% HNO_3 solution was then added to the flask and heated on a hot plate to boil. One to two hours was required for completed dissolution of the iron oxide film. The termination of the digestion was achieved when the beads appeared clean, without any yellow or brown color remaining on the surface, and the acid solution was clear to slightly yellow, without visible suspended particles. After cooling, 10 ml of the acid solution was filtered into another flask and diluted to 100 ml. This dilution was used to measure the total Fe content in the digested film by a Hach DR/2000 spectrophotometer at 562 nm using the FerroZine Method. The remaining acid solution was poured off and the beads were thoroughly rinsed by nanopure water. The flask with the beads was then baked at 300 °C for three hours before weighing again. The mass of the iron oxide film per gram of the coated beads was calculated by the difference between the two weighing results.

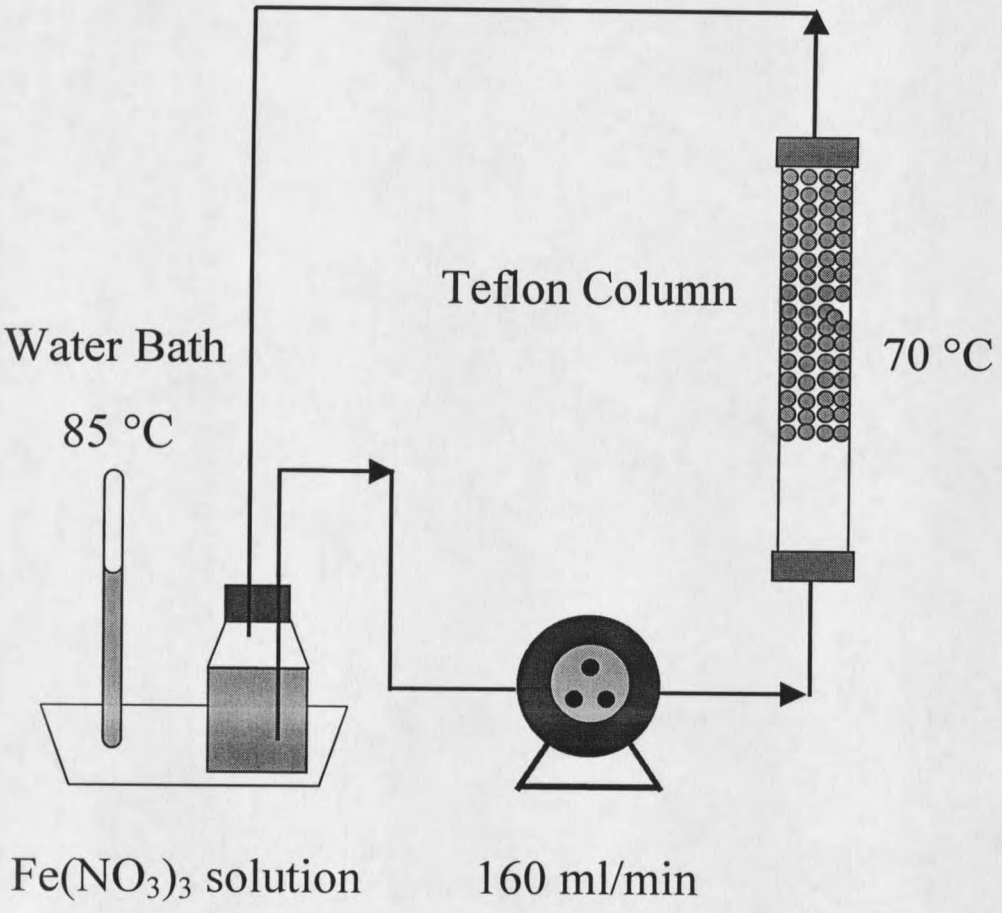

Figure 4. Schematic of iron oxide coating process on micro glass beads.

Stability of the Iron Oxide Film

The stability of the goethite film was estimated by the quantity of Fe that would redissolve in aqueous solution during the adsorption experiment. It was determined by adding 15 g of the coated beads to a 100 ml glass bottle (Pyrex) containing 60 ml of nanopure water with pH buffered to 7.4. The bottle was shaken for 24 hours. The solution was then filtered through a 0.2-μm nylon syringe filter (Fisher Scientific). A Hach DR/2000 spectrophotometer was used to determine the total iron concentration in the water solution at 562nm using the FerroZine method.

X-ray Photoelectron Spectroscopy (XPS)

The elemental content of the iron oxide film surface was determined by X-ray Photoelectron Spectroscopy (XPS). A Physical Electronics Laboratories PHI-5600 ESCA spectrometer was used for the analysis. A monochromatic Al K^{α} source (1486.6 eV) was operated at 350 watts (15 KV, 23.3 mA). The samples were analyzed at a 45° take-off angle that equated to a sampling depth of approximately 60 Å. The entrance aperture at the hemispherical energy analyzer was set at 4. Pass energies for the analyzer were set at 93.90 eV for wide region survey scans and 58.70 eV for elemental multiplex scans of C1s, O1s, Fe2p and Si2p. The operation pressure inside the main chamber was typically 5 x 10^{-8} torr. PHI ACCESS software was employed to collect the data and to calculate the atomic concentration from peak area.

Atomic Force Microscope (AFM)

Images of the iron oxide film surface were obtained with a Dimention 3100 Scanning Probe Microscope (Digital Instrument), which performs TappingMode Atomic Force Microscopy (AFM). The sample was attached to the top of a sample disk with double-sided tape. Vacuum chucks were used to hold the sample disk on the X-Y stage. TappingMode AFM operates by scanning a silicon tip integrated to the end to an oscillating cantilever across the sample surface. The cantilever was oscillated at or near its resonance frequency with amplitude ranging typically from 20 nm to 100 nm. A feedback loop maintained a constant oscillation amplitude and constant tip-sample interaction by maintaining a constant root mean square (RMS) of the oscillation signal acquired by a split photodiode detector. The vertical position of the scanner that was necessary to maintain the constant amplitude at each (x, y) data point was stored and analyzed by NanoScope IIIa controller and software Version 4.32r3 to make the surface images.

Surface Area Analysis

The specific surface area of the coated beads was determined using a Micromeritics Flowsorb II 2300 surface area analyzer, which employed the Brunauer-Emmett-Teller (BET) analysis method. The basic assumption of the method is that a monolayer of nitrogen gas molecules completely covers the sample surface at low temperature. 1 g of the coated beads was packed into a glass sample tube, and allowed to degas at 150 $^{\circ}$C for 20 minutes. Then the

sample tube was immersed in a liquid nitrogen bath (about -200 °C), and a flow of nitrogen gas mixed with an inert carrier gas (helium) was passed through the tube under ambient pressure. By monitoring the nitrogen content in the influent and effluent of the sample tube, the surface area of the beads could be calculated from the amount of nitrogen adsorbed. A three-point measurement was applied.

Adsorption and Desorption Experiments

Humic Stock Solution

The humic substances sample used in this experiment and in the growth experiment were extracted by alkali from Elliot Silt Loam Soil (ESLS) obtained from the International Humic Substances Society (IHSS), and without further treatment. 50 g of the soil sample was added to 1 L of 0.1 N NaOH solution, mixed for 24 hours, and then centrifuged at 10,000 rpm at 4 °C for 15 minutes to remove solid particles. The concentration of the humic substances in the solution was measured as total organic carbon. The solution was stored in the dark at 4 °C.

Glassware Cleaning Procedure

All glassware used in this experiment, including the TOC auto sampling vials, was acid washed for 12 hours, and rinsed 6 times with nanopure water. The glassware (except the volumetric flasks and pipettes) was then covered in

foil and baked at 300 °C for at least 8 hours. The glassware was removed from the oven and the foil was tightened prior to storage.

pH Buffering Method

The adsorption of humic acid by iron oxides is significantly pH dependent, and the consumption of carboxyl acid groups usually increases the pH of the solution during the process (Parfitt et al., 1977). To maintain a constant pH during the adsorption experiment, a proper pH buffering method was necessary. The usual phosphate buffer solution (PBS) could not be used in our case, since the phosphate ion would competitively react with the hydroxyl group on the iron oxide surface and prevent the adsorption of humic acid (Gu et al., 1994). A CO_2/N_2 gas mixture was used to solve the problem. High purity CO_2 and N_2 (Air Liquide America Corp.) were allowed to bubble through sample solution. The pH of sample solution was monitored by a pH meter (PerpHecT model 310, ATI Orion). Two variable area flowmeters (Cole-Parmer) and gas regulators were used to adjust the flow rates of both gases, and subsequently adjust the solution to a desired pH. The gas stream was continuously bubbled through the solution with rapid mixing until a stable pH was achieved for 20 minutes. The sample was then pipetted to the reaction bottle. The bottle was sealed and was only opened to add coated beads. Two pH values of 6.7 and 7.6 were used during the adsorption experiments. After the adsorption process, the pH values of these solutions were measured again to evaluate the buffering effect.

Adsorption Procedure

Goethite and hematite have very strong adsorption affinities to humic substances. Gu et al. (1994) reported that the adsorption was complete within minutes. Tipping (1980) found that the adsorption reached its equilibrium within 16 hours.

The sample solutions were prepared by diluting the humic stock solution to the desired TOC concentration with nanopure water. For the experiments at pH of 6.7, a total of 23 sample solutions were prepared with different TOC concentrations in the range of 0 - 50 ppm C. For the experiments at a pH of 7.4, a total of 25 solutions were prepared with different TOC concentrations. 200 ml of each sample solution was buffered to the desired pH. Then it was pipetted into three 100-ml reaction bottles (glass, Pyrex); each held 60 ml of the sample solution. About 15 g of goethite coated beads were accurately weighed and added to the first two reaction bottles for duplicate measurements. The other bottle of the same sample solution was for the control measurement (without beads). All the bottles were tightly closed and shaken for 24 hours. After 24 hours, TOC measurements of the solutions were taken as described in the following section. The adsorption of the ESLS humic substances on the created iron oxide surfaces was calculated by the difference between the TOC concentrations of the reaction solution and the control solution.

Desorption Test

The adsorption of humic acid on the iron oxide/water interface is a thermodynamically reversible reaction. The desorption process is usually coupled with the adsorption. The desorption test was performed to estimate the stability of the adsorbed humic substances at the iron oxide/ water interface.

The desorption test was performed for the last 23 sample solutions at pH of 7.4 with two repeat experiments for each solution. The adsorption in the first two sample solutions was too low to obtain a measurable desorption. After the adsorption experiment, the sample solutions in both reaction and control bottles were poured off and the bottles and beads were rinsed three times with 40 ml of nanopure water. Then 60 ml of pH-buffered nanopure water was pipetted into both bottles. The bottles were tightly closed and shaken for 48 hours. TOC measurements were then taken as described in the following section. The desorption of the adsorbed ESLS humic substances on the created iron oxide surfaces was calculated by the difference between the TOC concentrations of the reaction solution and the control solution.

Total Organic Carbon (TOC) Measurement

Samples for TOC were taken from the reaction and control bottles and immediately diluted to less than 2 ppm with nanopure water. 30 ml sterile, disposable syringes (Beckton Dickinson) and sterile 0.2-μm nylon syringe filters (Fisher Scientific) were used for the process. Both the syringes and the filters were prewashed with 30 ml of 0.1N HCl followed by 120 ml nanopure water. The

first 10 ml of the filtered sample solution were wasted. All TOC samples were acidified prior to analysis using 0.2 ml of 2N HCl per 40 ml of sample or its appropriate dilution. The samples were analyzed for non-purgeable organic carbon (NPOC) using a Shimadzu TOC 5000A analyzer with high sensitivity catalyst and an auto sampler. Standard curves for the TOC 5000A were developed using 4 concentrations of potassium hydrogen thalate. The resulting calibration curve typically had a coefficient of determination (R^2) in range of 0.98 to 1.00. An internal standard (same as the standards used to develop the calibration curve) was always run with each group of samples to correct for any variations in carrier gas flow rate.

Biofilm Growth Experiments

Flow Cell and System Configuration

A parallel plate flow cell was used to estimate the biofilm growth behavior on the iron oxide surface. The common flow cell design used by the Center for Biofilm Engineering was employed and is shown in Figure 5. A flow chamber (1 inch $\times$ 1 inch $\times$ 1 mm) was made on the polycarbonate base with 60° entrance angle on both the inlet and outlet side. The entrance angle was necessary to reduce side effects and turbulence of the flow in the chamber. The influent and effluent of the flow were introduced through two aluminum tubes. The goethite coated glass coverslip was held on the flow cell base by a silicon rubber gasket and an aluminum cover with screws and nuts.

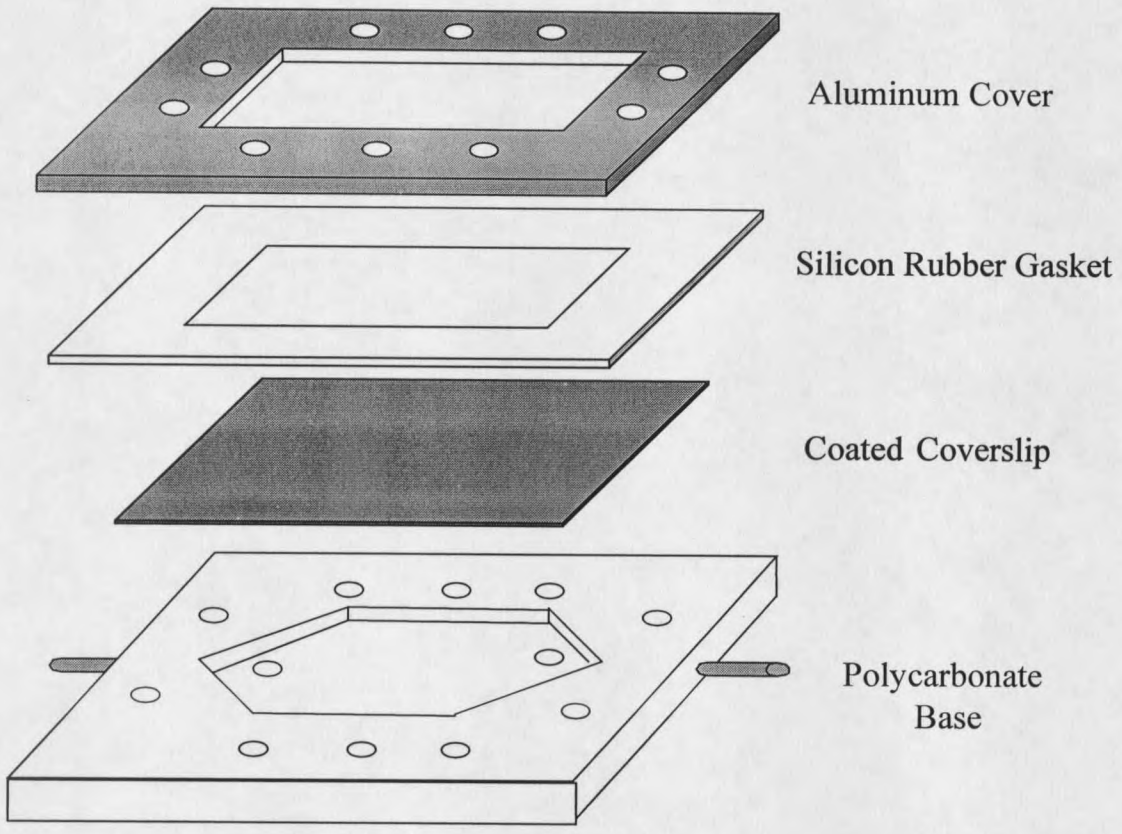

Figure 5. Schematic of the flow cell.

Figure 6 shows a schematic of the entire flow cell system. The system consists of the media and waste containers, flow cell, peristaltic pump, air catching vessel, inoculation site, and tubing (MASTERFLEX, size 14, Cole-Parmer) and connectors. To prevent any air bubbles in the system, the pressure in the flow chamber had to be maintained higher than the atmosphere, so the flow cell was operated below the solution level in both the media and the waste container (the dashed line in Figure 6), and the flow rate in the system was carefully set at 2 ml/min.

Any air bubbles accidentally entering or generated in the system could be caught by the air catching vessel prior to the flow cell. This was very important to the experiment since the air bubbles, once in the flow cell, would stay on the coverslip surface and prevent the biofilm cells from contacting the media. This vessel also reduced the pulsing effect from the peristaltic pump. The entire system was assembled on a cart so that it could be moved to and from the microscope.

A chemostat system shown in Figure 7 was used to culture the cells needed to inoculate the flow cell system. The system included a 450-ml working volume chemostat with media and waste containers. Air was bubbled into and out of the chemostat through 0.2-μm air vent filters.

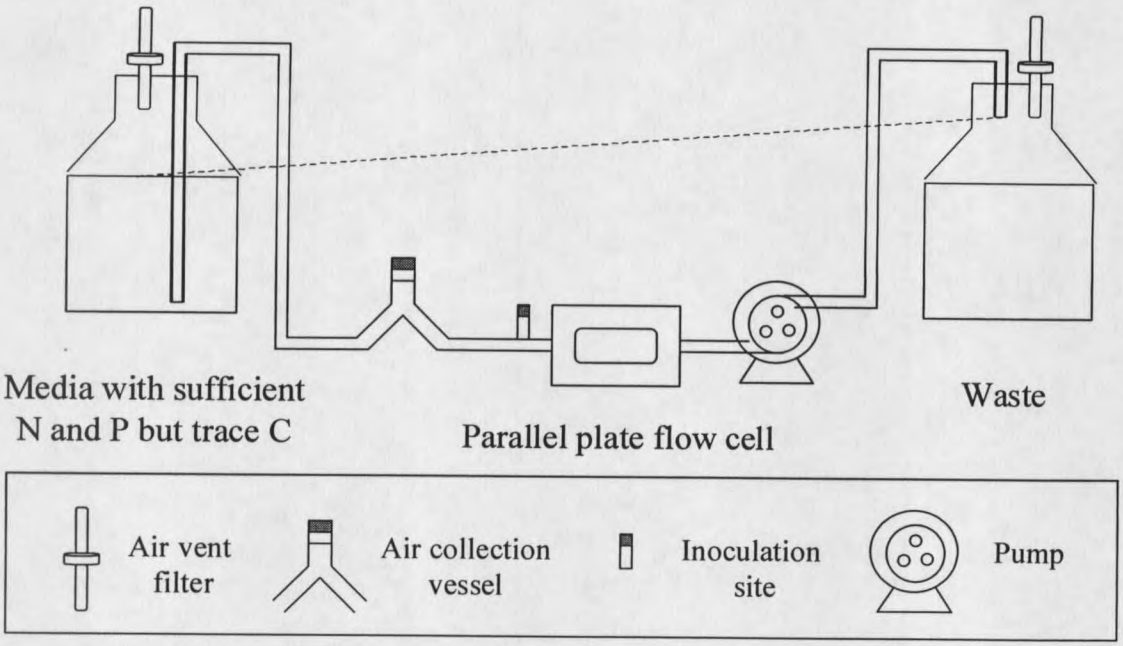

Figure 6. Schematic of the flow cell system (The flow cell should always be operated under the water level line to prevent the occurrence of air bubbles)

Organism

A culture of *Pseudomonas aeruginosa* (PAO1, GFP+, Department of Microbiology, Montana State University) was used for the growth experiment. The GFP gene on the pMF36 plasmid within the cell would synthesize green fluorescent protein that would produce fluorescence under proper UV light. This made it possible to do the real time mircoscopy to monitor the accumulation of the cells on the lower surface of the coverslip of the flow cell without staining. A frozen culture of the bacteria was streaked for isolation on plates of R2A agar (Difco, Inc.) with 150 mg/L carbenicillin (Sigma). The plates were incubated for 24 hours at 35 °C. One colony from an uncontaminated plate was then streaked on another R2A plate and incubated to make a confluent lawn. The cells were then collected and stored in a 20% glycerol and 2% peptone solution at –70 °C. the frozen stock culture was used as an inoculum for the chemostat culture.

Cleaning and Sterilization

The chemostat system and the flow cell system (except the flow cell) was assembled and rapidly flushed with nanopure water for two hours. The assembled components were autoclaved for 20 minutes at 121 °C and 23 psi pressure with the tubing ends wrapped by aluminum foil and autoclave tape.

The flow cell parts (except the coated coverslip) were washed thoroughly with antibacterial soap, rinsed with nanopure water several times and allowed to dry in air. Just before the experiment, the polycarbonate base was soaked in 70% ethanol for 30 minutes, then was placed under UV light in a hood for 30

minutes and allowed to air dry before assembly. The aluminum cover, rubber gasket, screws and nuts were wrapped in aluminum foil and autoclaved for 20 minutes at 121 °C and 23 psi pressure, and placed in the hood under UV light 20 minutes before assembly.

Media

Different media were used for the chemostat culture and the flow cell operation. The composition of the chemostat culture media is listed in Table 2. The humic substances were diluted from the humic stock solution, and adjusted to neutral pH by adding concentrated HCl. This diluted humic solution was used as the only carbon source for the cells in the chemostat. This procedure examined the planktonic cell growth potential of *Pseudomonas aeruginosa* (PAO1, GFP+) on this carbon source, and ensured that the cells had become physiologically adapted to this carbon source. The media was prepared in a 9 L carboy and autoclaved at 121 °C and 23 psi pressure for 15 minutes per liter.

Table 2. Chemostat culture media composition.

Component	Amount per liter media
K_2HPO_4 (Fisher Scientific)	0.70 g
KH_2PO_4 (Fisher Scientific)	0.30 g
$(NH4)_2SO_4$ (Fisher Scientific)	0.10 g
Humic Substances	100 mg

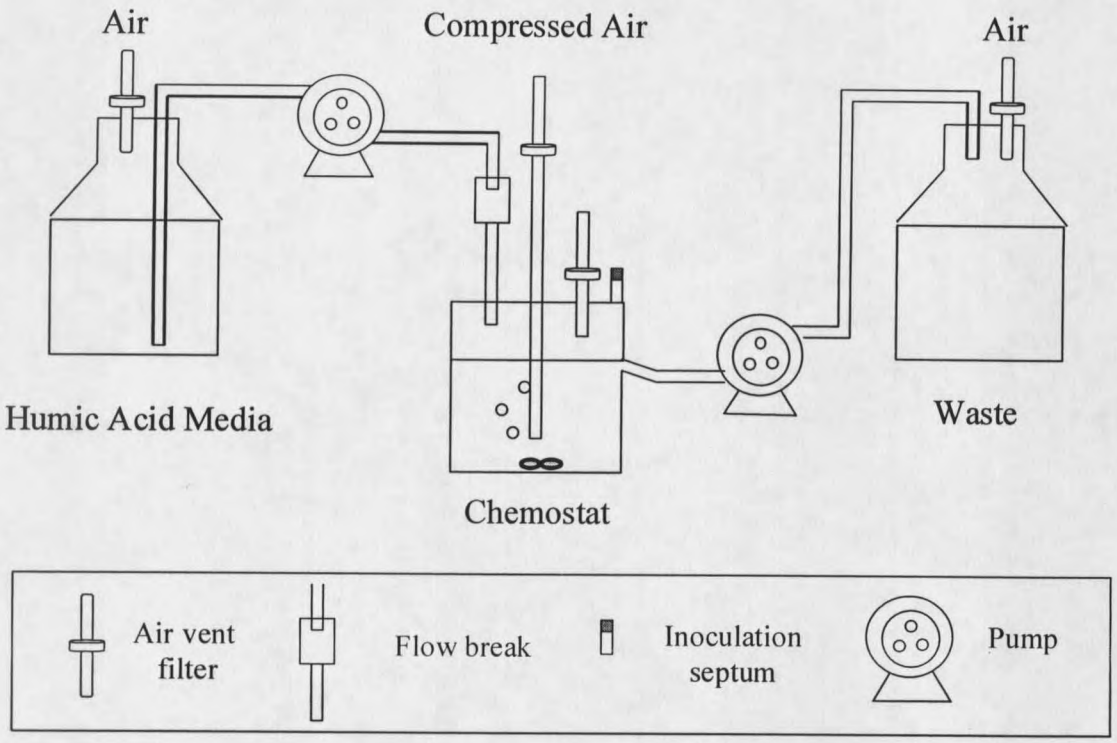

Figure 7. Schematic of the chemostat system

The composition of the flow cell media 1 and the concentrations of the nutrients are listed in Table 3. There was less than 100 ppb of organic carbon in the media. This composition ensured that the organic carbon was the growth-limiting nutrient. The bicarbonate salt was used to buffer the media at a defined CO_3^{2-} concentration and pH. KNO_3 and K_2HPO_4 were first dissolved in nanopure water in a 20-L carboy. The pH of the solution was adjusted to 7.2 to 7.4 with concentrated HCl. The solution was then autoclaved at 121 °C and 23 psi pressure for 15 minutes per liter. After cooling, $KHCO_3$ was dissolved in 10 ml nanopure water, adjusted to pH around 7.4, and injected into the carboy through a 0.22-μm syringe filter to make the final media.

Table 3. Flow Cell Media 1 Composition.

Component	Amount per liter	Nutrient concentration
KNO_3	2.9 mg	0.4 mg/L N
K_2HPO_4	0.2 mg	0.04 mg/L P
$KHCO_3$	0.2 g	100 mg/L eq. $CaCO_3$

A second flow cell media was also used during the growth experiment. This media had the same compositions as the flow cell media 1 except that 0.25 mg C/L ESLS humic substances was added.

Chemostat Culture

The *Pseudomonas areuginosa* was cultured in the sterile 450-ml chemostat to produce an inoculum for the flow cell system. The chemostat was first filled with the chemostat media to its working volume and the flow pump was then

turned off. 0.5 ml frozen stock of the *Pseudomonas aeruginosa* was warmed to room temperature and injected into the chemostat through the septum at the top. Air was then allowed to bubble into the media through 0.2-μm air vent filters. The media was mixed continuously using a stir plate. The bacteria were first cultured in batch mode. 1 ml of the culture was taken every 2 hours for total direct cell counts. After the cell number attained a maximum value and was unchanged for 15 hours, the flow pump was turned on again at a rate of 1.5 ml/min, which gave a 5-hour residence time. The media was allowed to overflow to waste. The bacteria were grown in continuous culture for 48 hours before the flow cell system was inoculated.

Total Direct Cell Counts (TDC)

The total direct cell counts method was used to monitor the growth of the bacteria in the chemostat culture using humic acid as the carbon source. 1 ml of the chemostat culture was sampled and added into a sterile test tube containing 9 ml of sterile water to make a 10^{-1} dilution. The mixture was vortexed for 1 minute. Further dilutions were prepared by repeating the same procedure. Cell counts were performed immediately after sampling. 1 ml of each dilution was filtered onto 0.2-μm pore size black polycarbonate filter (Millipore). Total cell counts were then obtained using a Nikon Eclipse 800 microscope with a B2A UV filter (450-490 nm Ex), and an ultra-violet source for epifluorescence of the sample. The proper dilution for the count was to have about 20 bacteria per field

(a 10 × 10-grid area on the ocular). 20 random fields per filter were selected. The total cell count per unit volume of the cell culture was calculated by Equation 15.

$$\text{total cell counts/ml} = \text{average cell count} \times \frac{\text{filter area}}{\text{field area}} \times \frac{\text{dilution rate}}{1\ \text{ml}} \qquad (15)$$

Adsorption Procedure of Iron Oxide Coated Coverslip

Two iron oxide coated coverslips were sealed in a beaker and autoclaved at 121°C and 23 psi pressure for 15 minutes. Then they were aseptically moved into two beakers in the hood. One beaker contained 200 ml autoclaved humic acid solution with low TOC concentration (12 ppm C for the first experiment, 5 ppm C for the other two experiments). The other beaker contained 200 ml autoclaved humic acid solution with high TOC concentration (66 ppm C for the first experiment, 50 ppm C for the other two experiments). The humic solutions were made by proper dilution of the humic stock solution, and adjusted to pH of 7.4. The beaker was sealed and the coverslip was equilibrated in the humic solution for 24 hours before the flow cell operation.

Flow Cell Operation

The sterilized flow cell parts were assembled under the hood. The goethite-coated coverslip was rinsed thoroughly with sterilized nanopure water before being placed on the base. The whole flow cell was slightly tightened by screws and nuts. Still under the hood, the flow cell was connected to the system tubing. The media was allowed to run through the whole system 15 minutes before inoculation.

A total of four flow cells were running simultaneously in each experiment. The first flow cell had an autoclaved pure glass coverslip. The second flow cell had an autoclaved iron oxide coated glass coverslip, but this coverslip was not pre-conditioned by the humic solution. The third flow cell had the iron oxide coated glass coverslip that had been equilibrated in the humic solution with low TOC concentration (12 ppm C for the first experiment, 5 ppm C for the other two experiments). The fourth flow cell had the iron oxide coated glass coverslip that had been equilibrated in the humic solution with high TOC concentration (66 ppm C for the first experiment, 50 ppm C for the other two experiments).

180 ml of the chemostat culture was taken by a 30-ml sterile, disposable syringe (Beckton Dickinson) and put into 6 sterilized 35-ml centrifuge tubes (Nalgene). The solution was centrifuged at 6,000 rpm at 4 $^{\circ}$C for 20 minutes. By aseptic operation, the solution was poured off. 20 ml of autoclaved flow cell media was added to each tube and vortexed for 2 minutes. The tubes were then centrifuged again at the same condition. The media was poured off. Another 10 ml of the media was added to each tube and vortexed for 2 minutes. Then the contents of all four tubes were mixed together and transferred into four 30-ml sterile, disposable syringes, which would be used to inoculate the four flow cells. Each syringe held 15 ml of the cell solution. Another 1 ml of the solution was diluted for total cell count.

The cell solutions were inoculated into the flow cells through the inoculation sites. The process was divided into three steps. In each step, 5 ml of

the solution was inoculated and the flow was stopped for 10 minutes to allow cells to adhere to the coverslip surface. After the inoculation, the flow was turned on and set at 2 ml/min with a Reynolds Number of 2.5 in each flow cell. This Reynolds Number assured a laminar flow in the flow cells. The flow cells were operated at ambient temperature. The number of cells on each coverslip was counted by real time microscopy every three to five hours.

During the last two experiments, after running the flow cell media 1 for about 24 hours, the pump was turned off. The carboy of the media was disconnected from the system in the hood. A carboy of flow cell media 2 was connected to the system. The connector on the carboy and the end of tubing were sterilized by 70% ethanol during the switching process. Then the pump was turned on again to 2 ml/min flow rate.

Real Time Microscopy

A Nikon Eclipse 800 microscope (1000x) with a B2A UV filter (450-490 nm Ex) was used for direct cell counts on each coverslip. The objective had a working distance of 0.13 mm, which was sufficient only to locate the bacteria attached on the lower surface of the coverslip. This was why a transparent coated coverslip was necessary for this experiment.

The first count was taken 1 hour after turning on the flow pump after inoculation. Only the permanently attached cells were counted. Cell counts were taken every three to five hours. At each time, 10 fields were randomly picked and

the cell number in each field counted. These fields were chosen near the center of the coverslip to avoid the possible edge effects.

Statistical Methods

The Adsorption Study

For the adsorption and desorption experiments, adsorption isotherms of the two different pH conditions were integrated from the adsorption data of ESLS humic substances to the created iron oxide surface by nonlinear least squares regression analysis using equation 12. A MATLAB (version 4.2c.1, The Mathworks, Inc.) program was written to calculate the nonlinear regression coefficients. The program is provided in Appendix B. The standard error of each coefficient of the isotherm was calculated by a bootstrap method (Efron and Tibshirani, 1993). The difference of each coefficient between the isotherms of the two pH conditions was compared by a two sample t-test.

The relationship between the desorption data and the respective adsorption data was analyzed by linear least squares regression using MINITAB software (version 12.1, Minitab, Inc.). The standard deviations of coefficients were also calculated.

The Biofilm Accumulation Study

The mean of the count on the surface at each time point was calculated and converted to $\log_{10}$ form. These data represent the biofilm density in the flow

cells. The results were plotted to show the differences between the experiments, flow cells, and the changes in time.

The biofilm accumulation was estimated by linear least squares regressions of the $\log_{10}$ form biofilm densities vs. time for each flow cell. The slope of each regression was calculated as the biofilm accumulation rate. A t-test was conducted for each slope to test the null hypothesis that slope = 0, which indicated no significant change of biofilm density and therefore no accumulation.

In the case that there was no significant change of biofilm density, the means of the biofilm density were compared among the flow cells using analysis of variance. In the case that there was significant change of biofilm density, the slopes were compared among the flow cells using the t-test.

The repeatability of the experiments was estimated by comparing the variance of the data for each experiment. All of these analyses were done in MINITAB and are provided in Appendix C.

CHAPTER 4. EXPERIMENTAL RESULTS

Introduction

This chapter presents the experimental results of this study. The characterization of the created iron oxide surface provides the physical, chemical and mechanical properties of the surface, which demonstrated the suitability of the surface for the subsequent adsorption research. The adsorption of the ESLS humic substances to the created iron oxide surface provides the modified Langmuir adsorption isotherms of two pH conditions. These isotherms were used to calculate the surface humic concentrations in the subsequent biofilm growth studies. The parameters of the model were also calculated and compared for different pH conditions. The desorption data were plotted vs. the respective adsorption data to demonstrate the stability of the adsorption.

The data of the attachment and the growth of *Pseudomonas aeruginosa* in the flow cells were plotted and compared for different experimental conditions, including the iron oxide coating, the humic substances pre-conditioning, and the media composition. These results were used to estimate the relationship between iron oxide surface humic adsorption and biofilm accumulation.

Characterization of the Created Iron Oxide Surface

As mentioned in Chapter 3, a layer of iron oxide was created on the surface of glass materials to simulate the iron corrosion products in natural environments. This iron oxide surface was used as the substratum for the subsequent humic adsorption studies and bacterial growth studies, where the knowledge of the physical, chemical, and mechanical properties of the surface is necessary.

The iron oxide coated glass beads were used to characterize the surface. A summary of some of the results is presented in Table 4.

Table 4. Characteristics of the iron oxide coated glass beads.

Characteristices of the coated beads	Specific amount per gram of coated beads
Coated material	1.246 ± 0.027 mg
Fe content in the coated material	0.258 ± 0.006 mg
Fe redissolved in the stability test	0.00374 ± 0.00019 mg
Surface area	0.1589 ± 0.0138 m^2

Digestion Test

The amount of coating material per gram of the coated beads as measured from the digestion test was 1.246 ± 0.027 mg, which was only 0.125% of the bead mass. Iron represents 20.7% of the total weight of the coating material and 0.0258% of the total weight of the coated beads. These low values suggested that a very thin film of coating material was established on the surface of the glass beads, and the density of the material may be low.

Stability of the Iron Oxide Film

The result of the stability test shows that less than 1.5% of the coated iron oxide would redissolve into the bulk solution under the conditions of the subsequent adsorption experiment. It was concluded that the adhesion of the iron oxide film to the glass beads surface was strong enough for the subsequent experiments.

XPS Analysis

Table 5 shows the atomic concentration of the created iron oxide surface measured by XPS analysis. Iron represents 19.3% of the surface, which concurred with the iron content as discussed previously. However, this value represents the atomic concentration of iron, and the digestion test calculated the weight concentration. If the higher atomic weight of iron was considered, the iron content on the surface, which was directly related to its adsorption capacity to humic substances, was higher than that inside the film. Table 5 also shows that the ratio of Fe concentration to O concentration on the surface was 0.483, which was very close to the Fe:O ratio (0.5) of goethite (FeOOH), suggesting that goethite was present on the surface.

The binding energy of the Fe2p electron of the surface is shown in Figure 8. The reference data is listed in Appendix A. The position of the Fe2p 3/2 peak was in the range of Fe_2O_3 (710.9 eV) and FeOOH (711.2 to 711.8 eV). It was not a single peak but a mixture of several peaks, which suggested that the surface contained different kinds of iron oxides, including FeOOH and Fe_2O_3.

Table 5. Atomic concentration of the iron oxide surface on glass beads (by monochromated Al Kα)

Element	Area (cts-ev/s)	Sensitivity Factor	Atomic Concentration(%)
Fe2p	133484	148.978	19.29
O1s	74035	39.890	39.95
C1s	25498	16.518	33.23
Si2p	5510	15.733	7.54

The binding energy of the O1s electron of the surface is shown in Figure 9. The position of the main peak was in the range of Fe_2O_3 (529.6 to 530.2 eV), suggesting that most of the oxygen atoms on the surface were combined with iron. There were also some small peaks in the range of 531 eV to 533 eV. These peaks might represent groups of nitrate (533 eV), carbonate (531 eV) or SiO_2 (533 eV). The data in Table 5 also show the occurrence of carbon and silicon. The large amount of carbon on the surface might be explained by the adsorption of CO_2 from air. The occurrence of silicon suggested that the glass bead surface was not fully coated, leaving some glass surface exposed. Thus, the atomic concentration of oxygen listed in Table 5 might exaggerate the actual amount of oxygen atoms on the film surface that were combined with iron, and the actural Fe:O ratio might be higher than 0.5.

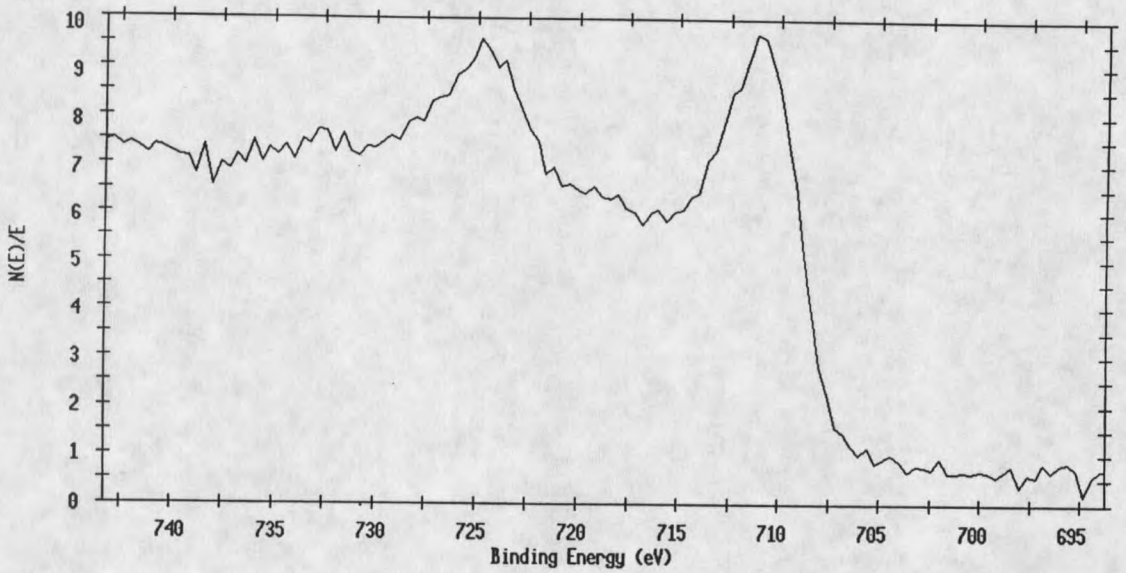

Figure 8. The binding energy of the Fe 2p electron of the created iron oxide surface measured by X-ray Photoelectron Spectroscopy.

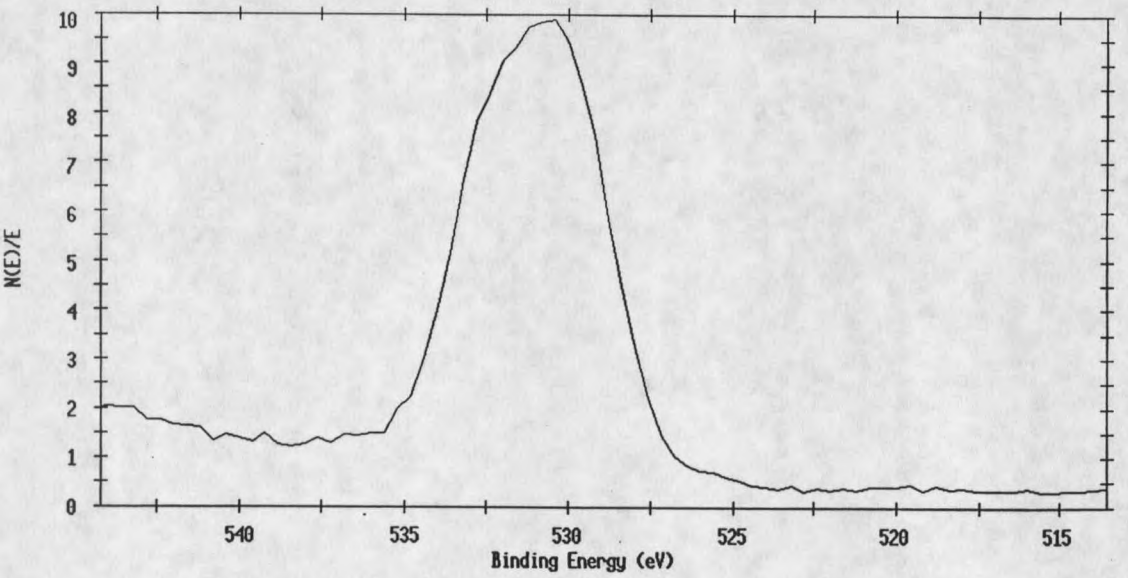

Figure 9. The binding energy of the O 1s electron of the created iron oxide surface measured by X-ray Photoelectron Spectroscopy.

AFM Analysis

AFM images of the iron oxide coated beads are shown in Figure 10. The top view shows that the bead was uniformly coated and had a relatively smooth surface. No cracks or pores were visible, except for some crystalline salt casts sized from 0.2 – 1.0 μm. These salt casts might be originally occupied by the unhydrolyzed ferric nitrate crystals, which were formed during the heating process and washed away by the subsequent rinsing. The surface view shows that very fine cone-like structures were formed throughout the surface. These structures demonstrated the domains of the iron oxide crystal nucleation and growth at each point. The sizes of these domains were usually from 40 nm to 100 nm, few exceeded 200 nm. These data also illustrated that the created iron oxide film was thicker than the sampling depth of XPS (60 Å), so the presence of silicon in Table 5 was not due to the detection of glass under the coating material.

Surface Area Analysis

The detailed data of the analysis are listed in Appendix A. The average specific surface area of the iron oxide coated beads, measured by the BET method, was 0.1589 ± 0.0138 m^2, only 48.2% higher than the surface area of the cleaned uncoated glass beads (0.1072 ± 0.000487 m2/g beads). The analysis also indicated that the formed iron oxide surface was non-porous and quite smooth. Since the sample used for the BET analysis was degassed at 150 °C, it is possible that the goethite in the sample surface might have been transformed

to a more oxidized structure, such as hematite, during the procedure, and it might still have retained a layer of adsorbed water molecules during the analysis. Thus, the BET analysis might not represent the actual surface area of the coated beads under normal water hydrated conditions.

Summary

The following characteristics of the iron oxide film established on glass surface by the method used in this study can be summarized. (1) A very thin film of iron oxide was formed on the glass surface. (2) This film contained a mixture of different iron oxides, dominated by goethite. (3) This film was very stable under the conditions of the subsequent adsorption experiment. (4) The glass beads were uniformly coated and the surface of iron oxide film is non-porous and smooth. Although the properties of the iron oxide film were measured from the coated beads, it was assumed that they also applied to the film on coated glass coverslip, since the same coating condition was used.

A. Top View

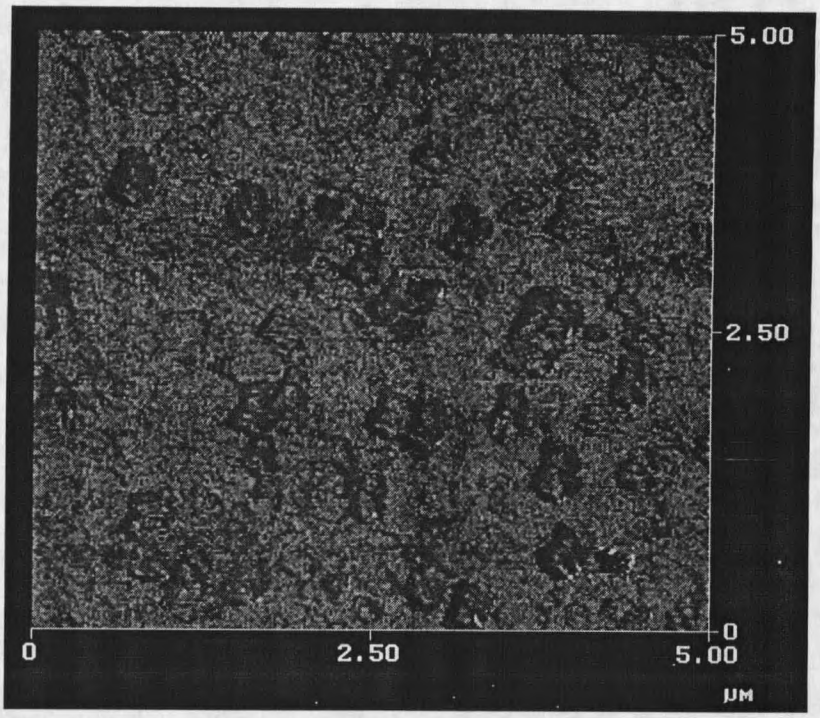

B. Surface View

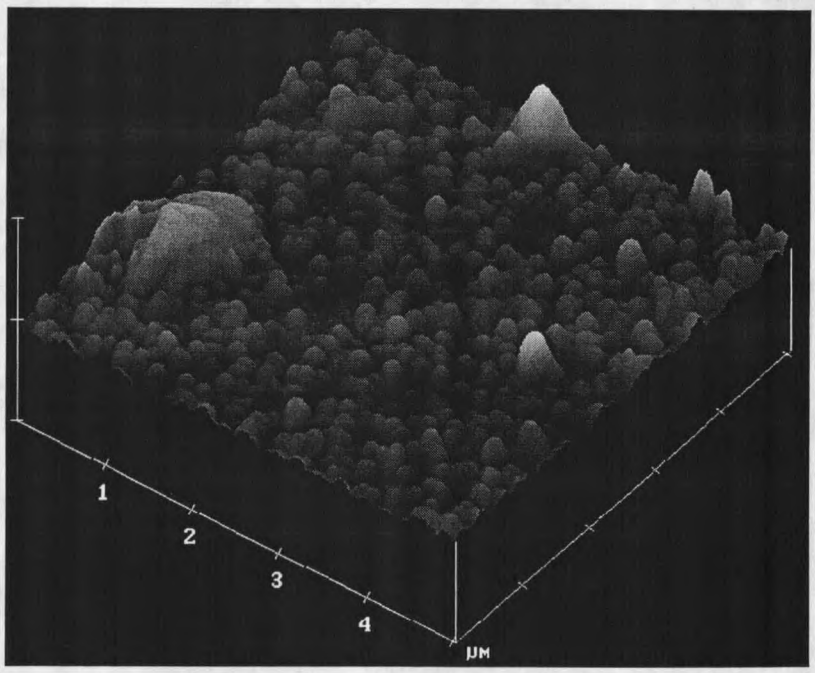

Figure 10. Images of the surface of the iron oxide coated glass beads by Atomic Force Microscopy.

Adsorption and Desorption of ESLS Humic Substance on the Created Iron Oxide Surface

In order to estimate the relationship between the adsorbed humic substances and the growth of bacteria on the created iron oxide surface, it is necessary to know how much humic substance was adsorbed. These data were obtained by the determining the adsorption isotherm of our system.

Experimental Design

The experiment was performed in batch reactors where the iron oxide-coated beads were equilibrated with humic substance solutions. The humic solutions were buffered to the same pH value by bubbling CO_2/N_2 gas mixture through them. After the adsorption process, the pH values of these solutions were measured again. The results showed that the pH values of all the solutions increased about 0.2 units. This was due to the loss of CO_2 from the solutions during the operation and the consumption of acidic functional groups of the humic substances by the adsorption process. The results also showed that the differences of the final pH values among all the humic solutions were less than 0.05 pH, which indicated adequate capacity of the buffering method.

The adsorption of humic substances was measured for each humic solution as the difference of TOC concentrations between a reaction sample and a control sample. Both samples contained the same amount of the humic solution except that the reaction sample was mixed with the iron oxide-coated beads for 24 hours.

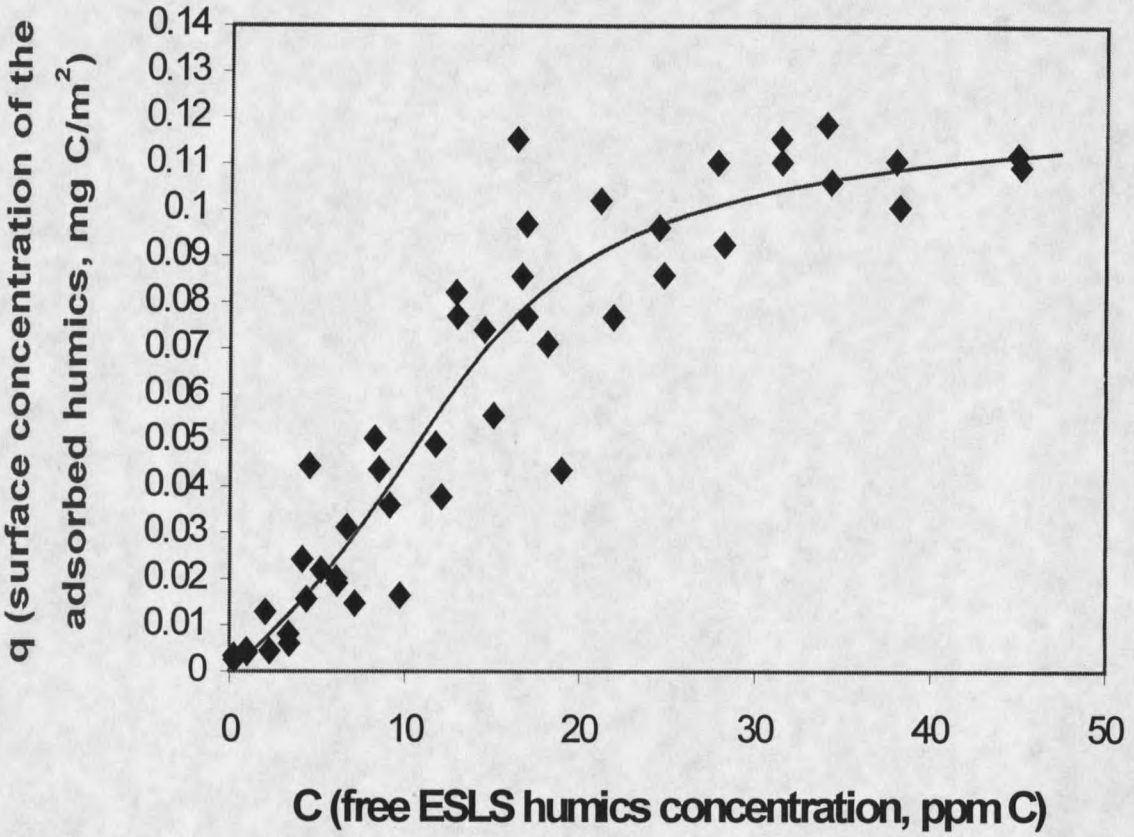

Figure 11. Adsorption results for ESLS humic substances on the created iron oxide surface at pH 6.7. The dots represent the experimental measurements. The solid line represents the adsorption isotherm of the modified Langmuir model simulated by non-linear least squares regression using a MATLAB program.

Adsorption Isotherm at a Neutral pH

The adsorption behavior under neutral pH was important to this study, as it is the common condition in natural aqueous environments as well as in water distribution systems. It is also a favorable condition for bacterial growth.

The adsorption data at the final pH of 6.7 is plotted in Figure 11. The X-axis presents the equilibrated free humic concentration in the bulk solution, determined by the final TOC concentration of the reaction sample. The Y-axis presents the adsorbed mass of humics per area of the iron oxide surface calculated from the adsorption value using the specific surface area of the beads. Figure 11 shows that at low free humic concentrations, the adsorption increased with an increase of the equilibrium bulk solution humic concentrations. As the free humic concentration exceeded 50 ppm of carbon, a plateau appears, indicating the existence of maximum adsorption.

Using the modified Langmuir model described in equation 12 and13, an adsorption isotherm of ESLS humic substances on the created iron oxide surface at pH 6.7 was simulated from the adsorption data by a non-linear least squares regression method, and is also showed in Figure 11. The calculated values of parameter q_{max}, K, and b for the model are listed in Table 6, along with their standard errors. These data indicated relatively high standard deviations for all of the parameters. Figure 11 also indicates that the measured data were scattered around the model isotherm. The estimated uncertainty of the parameters was due to the great possibility of experimental errors. As described in Chapter 3, the

humic sample solutions were filtered by syringe filters, and diluted by water before TOC measurements; both operations might introduce measurement errors. The accuracy of the Shimadzu TOC machine may also decrease after several measurements as the catalyst might accumulate iron or other metal elements from the sample solutions.

Table 6. Model parameters used in equation 13 and 14 to simulate adsorption isotherm data of ESLS humic substances on the created iron oxide surface at pH 6.7 and 7.4. Numbers in parentheses are standard errors. The p values were calculated by a t-test of each parameter with 43 degrees of freedom.

pH	q_{max} (mg/m^2)	K (m^3/g)	b (m^2/mg)
6.7	0.1263 (0.0083)	0.0261 (0.0043)	-8.4299 (2.1169)
7.4	0.1242 (0.0391)	0.0255 (0.0040)	-4.7165 (2.9554)
p	0.9592	0.9288	0.3128

The significance of the q_{max} and K values indicated that the modified Langmuir model fit well with the adsorption data in this study. However, the negative value of b implied that the adsorption energy decreased with the increase of the surface coverage, which was not consistent with the model.

pH Dependence of the Adsorption

As mentioned in Chapter 2, the adsorption of humic substances on the iron oxide surface is pH dependent. Thus, a study of the adsorption of the ESLS humic substances on the created iron oxide surface at different pH values was necessary for a good understanding of the adsorption process in the system as well as the biofilm accumulation behavior in the subsequent research.

To examine the pH dependence of the adsorption, another adsorption experiment was pursued at pH 7.4. The data were plotted in Figure 12 along with the adsorption isotherm simulated by the modified Langmuir model using the same non-linear least squares regression method. The isotherm had the same shape as that observed for pH 6.7, indicating the same adsorption mechanism in both conditions.

The values of three parameters of the modified Langmuir model at pH 7.4 were also listed in Table 6 along with their standard errors. These values were compared with those at pH 6.7 by a two sample t-tests of each parameter. The resulting p value for each parameter was also presented. The data show that both q_{max} and K values decreased with increasing pH. However, the differences were not statistically significant, since the differences were quite small and the standard errors of q_{max} and K values were relatively large.

The data in Table 6 also show a negative b value at pH 7.4, but the absolute value was smaller than that for pH 6.7. This suggests that the energy change during adsorption at pH 7.4 was not as significant as that at pH 6.7.

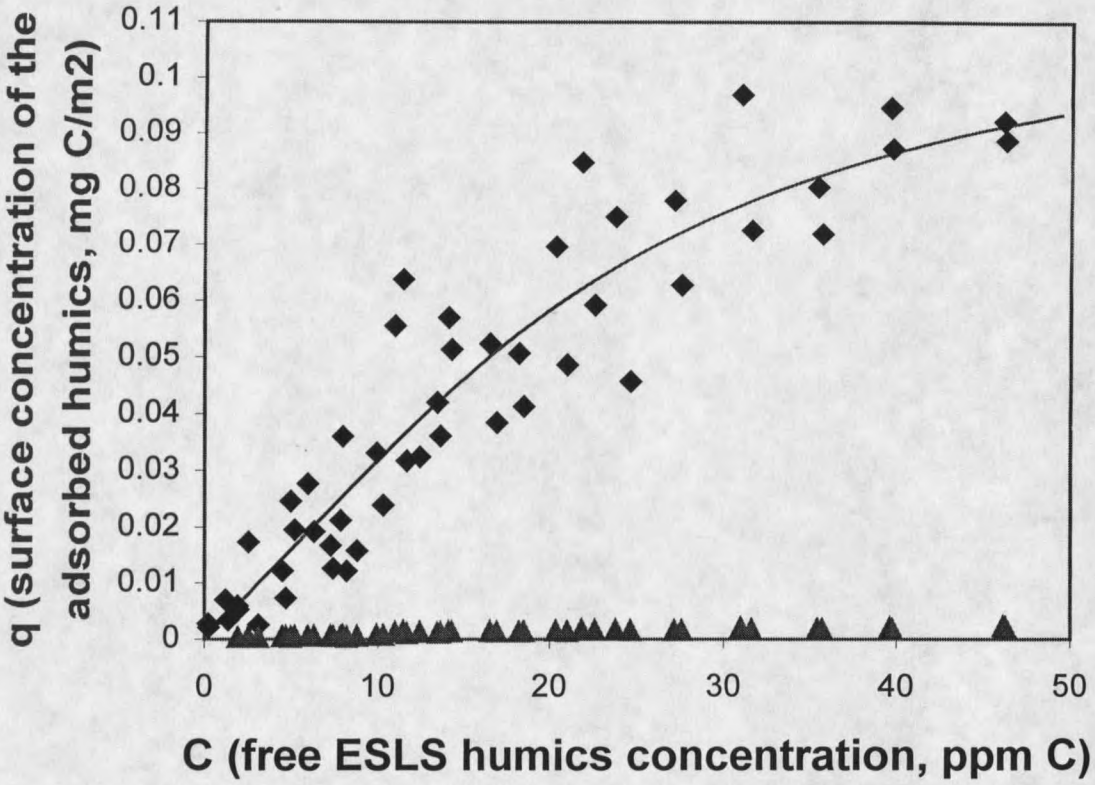

Figure 12. Adsorption and desorption results for ESLS humic substances on the created iron oxide surface at pH 7.4. The dots represent the adsorption measurements. The solid line represents the adsorption isotherm of the modified Langmuir model simulated by non-linear least squares regression using a MATLAB program. The triangles represent the desorption measurements corresponding to the free humics concentrations of the original adsorption equilibrium.

Desorption Potential

The adsorption of humic substances on iron oxide surfaces is thought to be thermodynamically reversible, although the desorption process has been studied to a much lesser extent than adsorption. The modified Langmuir model used in this study also considered that the already adsorbed humic substances desorb from the iron oxide surface back into the solution. If this desorption process occurs very fast at the water/solid interface, biofilm cells may have no chance to use the adsorbed humics as a carbon source for growth. Thus a desorption potential test for the stability of the adsorbed ESLS humic substances on the created iron oxide surface was necessary in this study.

The desorption test was conducted by equilibrating the iron oxide coated beads, which had already been allowed to adsorb the ESLS humics in the previously described adsorption experiment, with pH buffered TOC free nanopure water for two days. This longer test period was used to examine the stability of the adsorbed humics in a time period relevant to the subsequent biofilm growth experiments. The amount of desorption of the humics was estimated by the change of the TOC concentration of the water after the test.

The desorption potential of our system at pH 7.4 was tested immediately after the adsorption measurements at the same pH had been completed. The data of this test were also plotted in Figure 12 corresponding to the original equilibrated free humic concentrations of the sample solutions. Compared to the amount of the adsorbed humic substances on the surface, the desorption portion

was very small. The relationship between the amount of desorbed and adsorbed humic substances is shown in Figure 13, where the desorption data were plotted against the respective adsorption data.

Figure 13 shows that the amount of humic substances that desorbed from the iron oxide surface increased positively with the amount of the humics originally adsorbed on the surface. This trend could be well fit by a linear relationship (R^2 = 0.914). The slope of the line represents the average ratio of the desorbed to the adsorbed humic substances. The data indicated that, on average, less than 2.1% of the adsorbed humic substances desorbed from the solid surface back in to the liquid phase after two days of equilibration with TOC free water.

Summary

The results of the experiments discussed in this section showed that the ESLS humic substances could be significantly adsorbed on the iron oxide surfaces created in this study. The amount of adsorption increased with increasing free humics concentration in the equilibrated bulk solution until a maximum adsorption was reached when the free humic exceeded 50 ppm.

The adsorption isotherm for our system could be simulated using the modified Langmuir model. The calculated q_{max} and K values were positive while the b value was negative. Both the adsorption capacity and the affinity decreased with increasing pH of the sample solution, indicating a pH dependence of

adsorption. The desorption potential of the adsorbed humics from the iron oxide surface was very small, almost negligible compared to the adsorption capability.

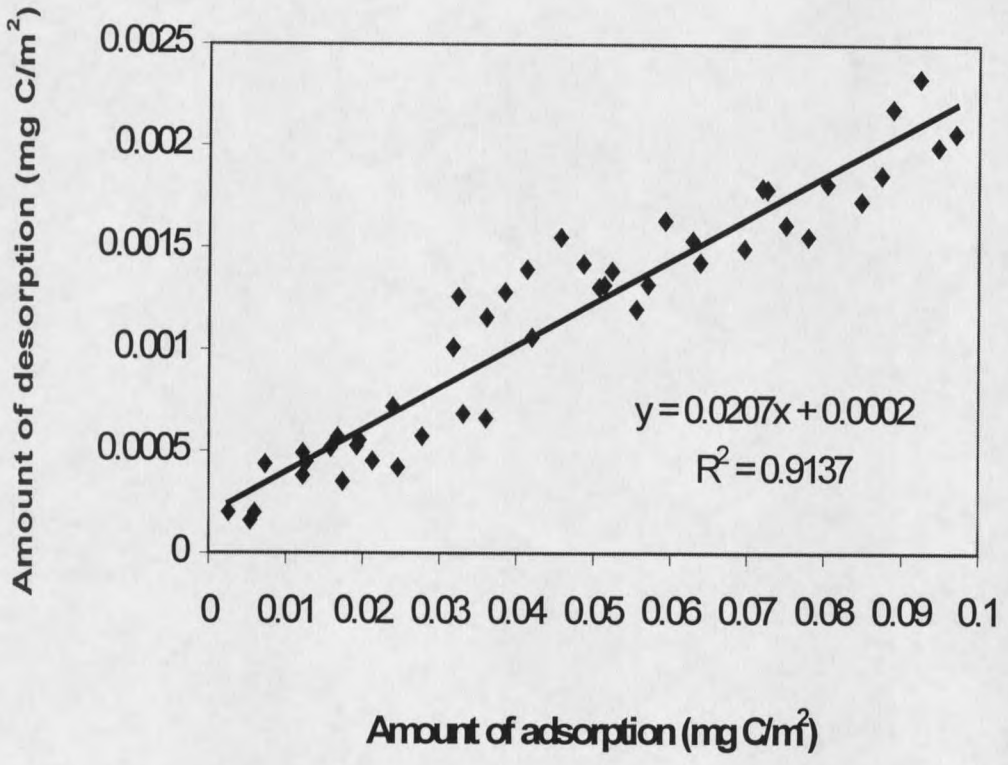

Figure 13. Relationship between the amount of the desorption of ESLS humic substances from the created iron oxide surfaces back into the water phase and the amount of the originally adsorbed humics on these surfaces. The dots represent the experimental data. The solid line represents linear regression by a least squares method in MINITAB.

Biofilm Accumulation on the Created Iron Oxide Surface with the ESLS Humic Substances Adsorbed

As described in Chapter 2, the surfaces of iron pipe lines in drinking water distribution systems support more biofilm accumulation than other materials. The bacterial colonization increases with the increasing potential of these surfaces to form iron corrosion products (mostly iron oxides). This effect is far more pronounced than what can be explained only by the disinfectant demand of iron and its corrosion products. It was hypothesized in this study that the adsorbed humic substances on iron oxide surfaces in drinking water distribution systems provide additional carbon and energy sources for biofilm growth. In order to test this hypothesis, studies of biofilm accumulation on the created iron oxide surface with the adsorbed ESLS humic substances was performed. The results are discussed in this section.

Experimental Design

The basic premise of the study was to measure the bacterial accumulation rate on the created iron oxide surface with the adsorbed humic substances as the only carbon source, and compare it with the accumulation rate on the surfaces without the adsorbed humics.

In order to observe the biofilm accumulation behavior in vivo, a GFP+ strain of *Pseudomonas aeruginosa* (PAO1) was used in the experiment. This microorganism produced green fluorescent protein, and the cells could be tracked under UV light without killing the cell by staining.

Four parallel plate flow cells were used simultaneously during the experiment. The first flow cell had a pure glass coverslip without iron oxide coating or humic pre-conditioning. It was used as a control to examine the significance of the effect of the iron oxide on the biofilm growth. The second flow cell had a glass coverslip coated with the iron oxide but without humic pre-conditioning. It was used as a control to examine the significance of the effect of the adsorbed humic substances on the biofilm growth. The third and fourth flow cells also had glass coverslips coated with the iron oxide, but with different amount of ESLS humic substances adsorbed on the surface. One coverslip was pre-conditioned in the range of low humic adsorption, another near the maximum adsorption, according to the adsorption isotherm presented in Figure 12. The biofilm accumulation rates on the coverslips of these two flow cells were compared to examine the significance of the effect of surface humic coverage on biofilm accumulation.

Two media, both with a pH around 7.4 and sufficient supplies of nitrogen and phosphorous, were allowed to run through the flow cells. Flow cell media 1 contained neither ESLS humic substances nor any other carbon source. It was used to demonstrate whether or not the adsorbed humic substances could support biofilm accumulation alone. Flow cell media 2 contained 0.25-ppm ESLS humic substances as the only carbon source. It was used to demonstrate if a continuous supply of adsorbed humics could enhance biofilm accumulation.

Chemostat Cell Culture

Before being inoculated into the flow cell system, the *Pseudomonas aeruginosa* was cultured in a chemostat system in planktonic phase. The media used for the culture contained 100 ppm ESLS humic substance as the only carbon source. There were two reasons to use this media. First, it was necessary to know if the bacteria could utilize the ESLS humic substances; second, it ensured that the bacteria would be physiologically adapted to this carbon source.

The chemostat was first operated in batch culture mode. Total direct cell counts were used to track the cell growth over time. The batch mode culture demonstrated three growth phases of the strain of *Pseudomonas aeruginosa* in the chemostat media as shown in Figure 14. The lag phase, in which the number of cells kept almost constant, continued for the first 40 hours of culture. Then the cell number started to increase logarithmly, indicating the rapid growth and proliferation of the bacteria. The cell number attained a maximum of about 5.1×10^8 cfu/ml at about 80 hour, then the stationary phase was observed.

At 100 hours running time the chemostat was switched to CSTR mode. The cell number in the reactor decreased rapidly due to flushing. The cell number became constant again after another 20 hours, indicating that all of the bacteria in the chemostat were forced to growth at the same rate of 0.2 hr^{-1} (5-hour residence time). Then the bacteria were ready to be inoculated into the flow cell system.

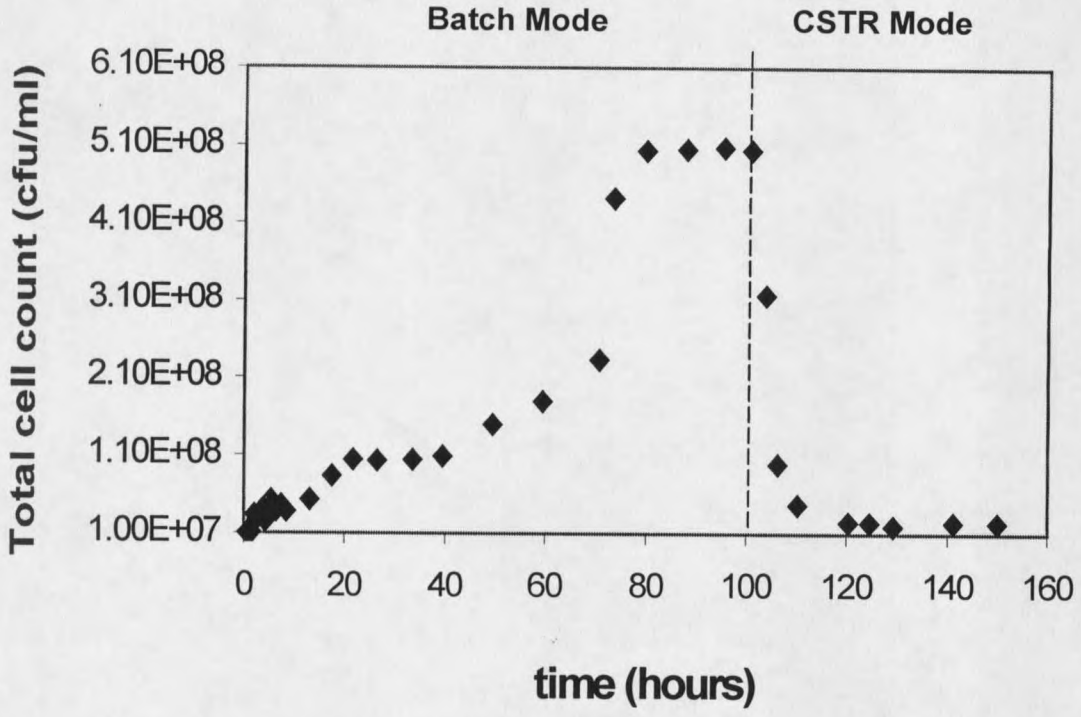

Figure 14. Chemostat culture of *Pseudomonas aeruginosa* (PAO1, GFP+) in a media with 100 ppm ESLS humic substances as the only carbon source. The culture was switched from batch mode to CSTR mode at 100 hours by turning on the pump to the flow rate corresponding to a 5-hour residence time.

The Biofilm Accumulation with Flow Cell Media 1.

Figure 14 demonstrates that the number of the *Pseudomonas aeruginosa* cells in the chemostat was constant 20 hours after turning the chemostat to CSTR mode. To ensure that all of the cells were in the same physiological growth phase, the chemostat was allowed to run in CSTR mode for 48 hours. The same amount of cells were harvested, washed, and inoculated into each of the four flow cells. Flow cell media 1 (no humics) was pumped through the flow cell chambers at the same laminar flow rate (2 ml/min). The numbers of the bacteria that attached to the lower surfaces of the coverslips were counted by real time microscopy.

Figure 15 shows the biofilm density on the coverslips of the four flow cells over the 140-hour experiment period. The symbols present the $\log_{10}$ values of the average cell counts of 10 random microscope fields. The coverslip in flow cell 1 was pure glass, while in flow cell 2, it was coated by the created iron oxide film. The coverslips in flow cell 3 and 4 were also iron oxide coated, and were pre-conditioned in 12 ppm and 66 ppm ESLS humic substances solutions respectively. According to the adsorption isotherm presented in Figure 12, the surface concentrations of the humics on these two coverslips were 0.0378 mg/m^2 and 0.1011 mg/m^2 respectively.

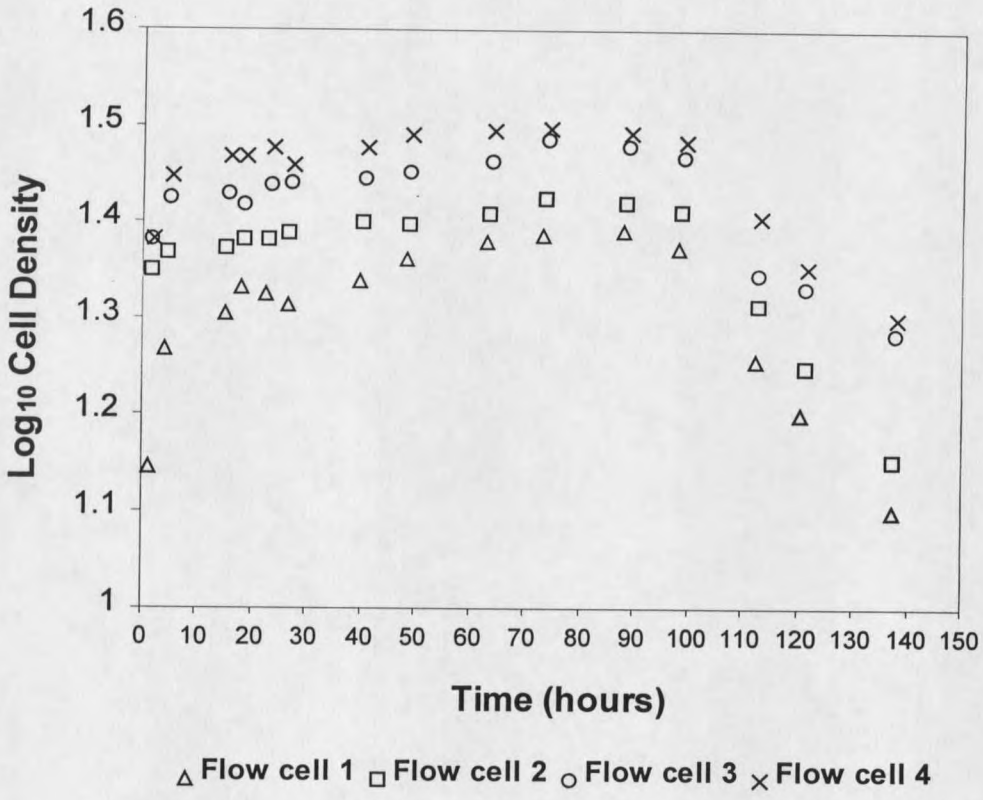

Figure 15. ***Pseudomonas aeruginosa*** **(PAO1, GFP+) biofilm accumulation on the coverslip surfaces of four flow cells using the flow cell media 1 with initial inoculation concentration of 4.02 $\times 10^6$ cfu/ml. The data points represent the $\log_{10}$ form of the average cell density on the surface. Flow cell 1 had a pure glass coverslip. Flow cell 2 had a glass coverslip coated with the created iron oxide. Flow cell 3 had an iron oxide coated coverslip pre-conditioned in 12 ppm ESLS humic substance solution. Flow cell 4 had an iron oxide coated coverslip pre-conditioned in 66 ppm ESLS humic substance solution.**

As shown in Figure 15, there were three periods of colonization of the biofilm. The first period began at time zero and continued for about 3 hours. In this period the cell numbers on the coverslips increased. However, no cell division was observed during this time by the real time microscopy, suggesting that the cells did not replicate.

The second period continued from 3 to about 95 hours. There were only slight changes of the bacterial cell numbers on the coverslips of the four flow cells during this period, which indicated that the biofilm densities in the flow cells were almost in a steady state phase. To estimate the significance of the biofilm accumulation in each flow cell during this period, the biofilm density data of each flow cell were integrated vs. time by a linear least squares regression in MINITAB. The slopes of the regressions represented the biofilm accumulation rates and are listed in Table 7 along with their standard deviations, the R^2 values of the regressions, and the p values calculated from t-tests to test the null hypothesis that the slopes were zero.

Table 7. The steady state phase accumulation rates of *Pseudomonas aeruginosa* (PAO1, GFP+) biofilm on the coverslip surfaces of four flow cells using the flow cell media 1. Calculated by linear least square regression of the data for each flow cell using MINITAB.

Flow cell	Mean of slope (hr^{-1})	Standard deviation	R^2	p
1	0.001357	0.000167	0.8914	0.0001
2	0.000683	0.000059	0.9443	0.0001
3	0.000787	0.000084	0.9165	0.0001
4	0.000849	0.000236	0.6304	0.0061

The p values in Table 7 indicate that all the slopes are statistically non-zero, which implies that significant biofilm accumulation existed in all the flow cells during this period. The R^2 values indicated that the accumulation were linear over time, except that in flow cell 4. The order of the accumulation rates in the flow cells was flow cell 1 > flow cell 4 > flow cell 2 > flow cell 3. Comparisons between these accumulation rates were made by two sample t-tests at $\alpha = 0.05$ level using MINITAB. The results are shown in Table 8, which demonstrated that the differences between flow cell 1 and all other flow cells were statistically significant, while the differences among flow cell 2, 3, and 4 were not significant.

Table 8. Comparison of the steady state phase accumulation rates of *Pseudomonas aeruginosa* (PAO1, GFP+) biofilm on the coverslip surfaces of four flow cells using the flow cell media 1. Calculated by t-tests at $\alpha = 0.05$ level using MINITAB.

Flow cell pair	1 - 2	1 - 3	1 - 4	2 - 3	2 - 4	3 - 4
p	0.0040	0.0132	0.0328	0.6450	0.3880	0.6950

Although the results in Table 7 showed statistically significant biofilm accumulation in all the flow cells, the magnitudes of the slopes, or the accumulation rates, were very small, especially when compared to the accumulation rates in the later experiments (will be discussed later). Furthermore, the observation of the biofilm cell division and movement was rare in all the flow cells during this period. Thus, there was great uncertainty of the significance of the biofilm accumulation during this period.

The average biofilm density in each flow cell during the second period is listed in Table 9 along with its standard deviation. Since all the biofilm densities changed over time, the average density in each flow cell was calculated as the value at the average time of this period, which was 40.4 hours. These average biofilm densities were compared to each other by calculating the Bonferrioni Pairwise Confidence Intervals for each pair of flow cells at α = 0.05 level using MINITAB. The results are shown in Table 10.

Table 9. The average *Pseudomonas aeruginosa* (PAO1, GFP+) biofilm densities on the coverslip surfaces of four flow cells using the flow cell media 1 at the steady state phase at the average time for all the flow cells (40.4 hours).

Flow cell	1	2	3	4
Average density	1.3396	1.3940	1.4473	1.4671
Standard deviation	0.0040	0.0040	0.0040	0.0040

Table 10. Comparison of the average *Pseudomonas aeruginosa* (PAO1, GFP+) biofilm densities on the coverslip surfaces of four flow cells using the flow cell media 1 at the steady state phase at the average time for all the flow cells (40.4 hours). Presented by the Bonferrioni Pairwise Confidence Intervals calculated at α = 0.05 level using MINITAB. The intervals are for (column level mean) – (row level mean)

Interval	Flow cell 2	Flow cell 3	Flow cell 4
Flow cell 1	0.07050, 0.12376	0.06930, 0.14355	0.03585, 0.08910
Flow cell 2	---	0.03840, 0.09165	0.03720, 0.11145
Flow cell 3	---	---	0.00374, 0.05700

These results indicated that during this period, the order of the biofilm densities in the four flow cells was flow cell 1 < flow cell 2 < flow cell 3 < flow cell 4. The differences were all statistically significant.

The third period of this experiment began at 95 hours and continued until the end of the experiment. The biofilm densities in all flow cells decreased continuously. The decrease rate in each flow cell was calculated as the slope of a linear least squares regression of the cell count data during this period over time. The slopes are presented in Table 11 along with their standard deviations, the R^2 values of the regressions, and the p values calculated from t-tests to test the null hypothesis that the slopes were zero.

Table 11. The decline phase decrease rates of *Pseudomonas aeruginosa* (PAO1, GFP+) biofilm densities on the coverslip surfaces of four flow cells using the flow cell media 1. Calculated by linear least square regression of the data for each flow cell using MINITAB.

Flow cell	Mean of slope (hr^{-1})	Standard deviation	R^2	p
1	-0.0069	0.0004	0.9930	0.0035
2	-0.0067	0.0002	0.9974	0.0013
3	-0.0045	0.0011	0.8853	0.0591
4	-0.0042	0.0009	0.9128	0.0446

The results of the p values indicated that the decrease of the biofilm densities in flow cell 1, 2, and 4 were statistically significant, while in flow cell 3, the decrease was not significant. All the decreases were linear over time. The order of the biofilm density decrease rates in the flow cells was flow cell 1 > flow cell 2 > flow cell 3 > flow cell 4. Comparisons between these decreased rates were made by two sample t-tests at $\alpha = 0.05$ level using MINITAB. The results are shown in Table 12, which demonstrates that the differences among all the

flow cells were not statistically significant, except that between flow cell 1 and flow cell 4.

Table 12. Comparison of the decline phase decease rates of *Pseudomonas aeruginosa* (PAO1, GFP+) biofilm densities on the coverslip surfaces of four flow cells using the flow cell media 1. Calculated by t-tests at α = 0.05 level using MINITAB.

Flow cell pair	1 - 2	1 - 3	1 - 4	2 - 3	2 - 4	3 - 4
p	0.8230	0.0607	0.0378	0.0870	0.0542	0.7643

Biofilm Accumulation with Flow Cell Media 2.

The data in Figure 15 did not provide clear and confident comparisons of the biofilm accumulations in the four flow cells, since the biofilm accumulation rates were too small. Supposing that the nutrient level was too low in media 1 to support the cell division, another experiment was completed. After running the flow cell media 1 through the system for a while, it was switched to the flow cell media 2, which contained 0.25 ppm of the ESLS humic substances. In this experiment, the coverslips of the first and second flow cells were still the same pure glass and the created iron oxide as for the previous experiment. The coverslips of the third and fourth flow cells were the created iron oxides pre-conditioned in 5 ppm and 50 ppm ESLS humic substances solutions respectively. Calculated from the adsorption isotherm presented in Figure 12, the surface concentration of the humics on these two coverslips were 0.0161 mg/m^2 and 0.0939 mg/m^2 respectively. Although these surface concentrations were slightly

different than that used in the previous experiment, they were still in the same range where a low coverage and a nearly maximum coverage applied.

Two separate replicates were completed. The biofilm density data vs. time were plotted in Figure 16 and Figure 17. Again, these data represented the average cell counts of 10 random microscope fields, and were transformed to the logarithm form.

Results with Flow Cell Media 1. Figures 16 and 17 show that, before switching the media, the biofilm cells in all the flow cells had the same trends of behavior as the previous experiment with flow cell media 1 alone. Two periods existed before switching the media. Up to three hours after the inoculation, the cell numbers on all the coverslips increased, but cell division and proliferation was not observed. After three hours, a steady-state phase appeared where the biofilm density in the flow cells did not change. As in the previous experiment, the biofilm density data from each flow cell were integrated vs. time by a linear least squares regression in MINITAB to estimate the significance of the biofilm accumulation in each flow cell during this period. Representing the biofilm accumulation rates, the slopes of the regression lines are listed in Table 13 and Table 14 for the two replicates. Their standard deviations, the R^2 values of the regressions, and the p values calculated from t-tests are also presented.

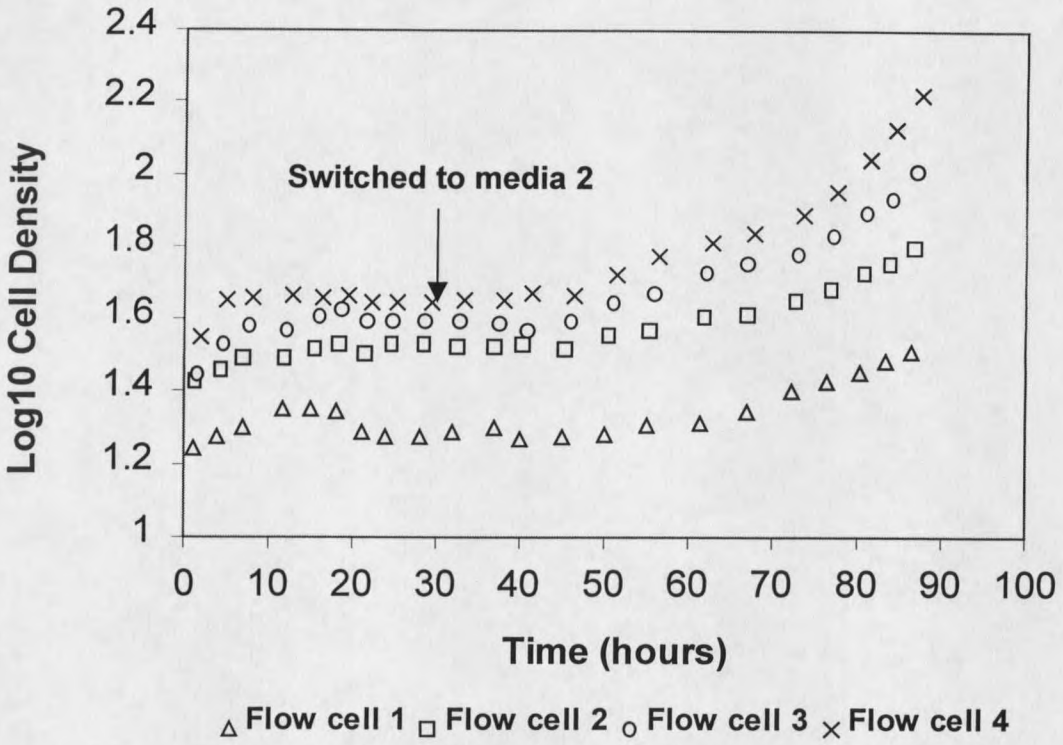

Figure 16. ***Pseudomonas aeruginosa*** **(PAO1, GFP+) biofilm accumulation on the coverslip surfaces of four flow cells using the flow cell media 1 and media 2 (replicate 1) with initial inoculation concentration of 5.97 $\times 10^6$ cfu/ml. The data points represent the $\log_{10}$ form of the average cell density on the surface. Flow cell 1 had a pure glass coverslip. Flow cell 2 had a glass coverslip coated with the created iron oxide. Flow cell 3 had an iron oxide coated coverslip pre-conditioned in 5 ppm ESLS humic substance solution. Flow cell 4 had an iron oxide coated coverslip pre-conditioned in 50 ppm ESLS humic substance solution.**

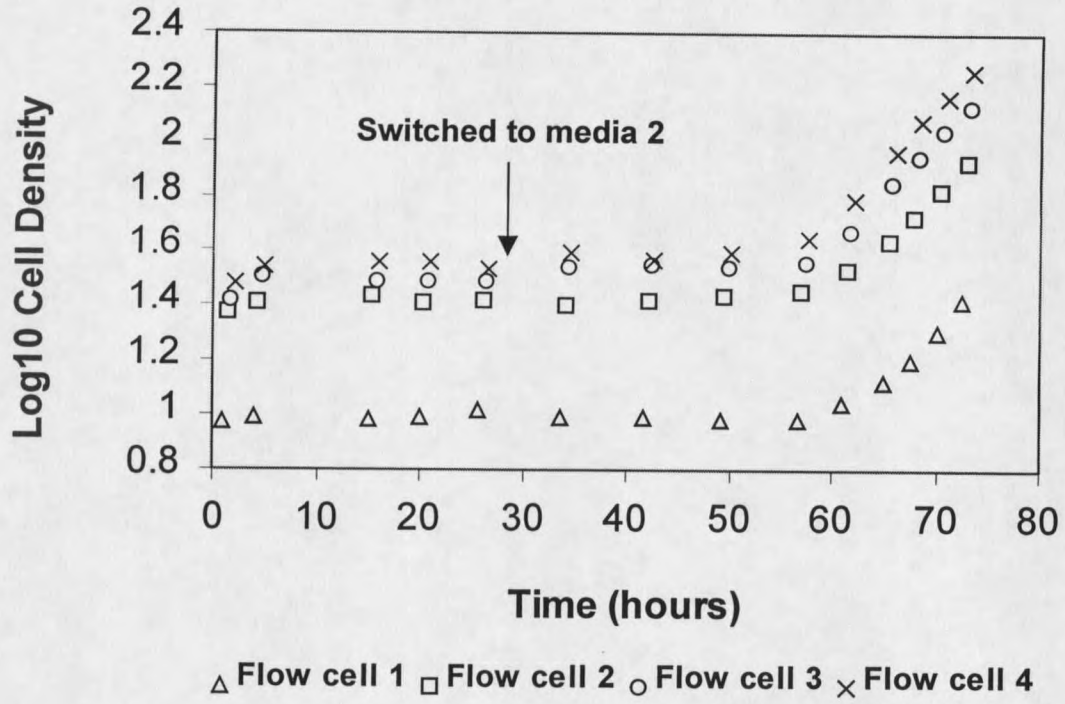

Figure 17. The repeat experiment of *Pseudomonas aeruginosa* (PAO1, GFP+) biofilm accumulation on the coverslip surfaces of four flow cells using the flow cell media 1 and media 2 (replicate 2) with initial inoculation concentration of 4.77×10^6 cfu/ml. The data points represent the $\log_{10}$ form of the average cell density on the surface. Flow cell 1 had a pure glass coverslip. Flow cell 2 had a glass coverslip coated with the created iron oxide. Flow cell 3 had an iron oxide coated coverslip pre-conditioned in 5 ppm ESLS humic substance solution. Flow cell 4 had an iron oxide coated coverslip pre-conditioned in 50 ppm ESLS humic substance solution.

The values of the slopes in Table 13 and 14 show that the biofilm accumulation rates in all the flow cells in both replicates before adding of 0.25 ppm C humics were very small, and of the same magnitude as the results of the previous experiment in which only the flow cell media 1 was used. The results of the p values indicated that during the steady state phase in both of the replicates, none of the flow cells demonstrated statistically significant biofilm accumulation. The exception is the flow cell 2 in the first replicate, in which the biofilm accumulation was significant at the 0.05 level. The R^2 values indicated that in both replicates none of the biofilm accumulation was linear.

Table 13. The steady state phase accumulation rates of *Pseudomonas aeruginosa* (PAO1, GFP+) biofilm on the coverslip surfaces of four flow cells before switching the media in the replicate 1. Calculated by linear least square regression of the data for each flow cell using MINITAB.

Flow cell	Mean of slope (hr^{-1})	Standard deviation	R^2	p
1	0.002585	0.001348	0.3800	0.103
2	0.001349	0.000528	0.5210	0.043
3	0.000703	0.000815	0.1100	0.422
4	0.000576	0.000323	0.3450	0.126

Table 14. The steady state phase accumulation rates of *Pseudomonas aeruginosa* (PAO1, GFP+) biofilm on the coverslip surfaces of four flow cells before switching the media in the replicate 2. Calculated by linear least square regression of the data for each flow cell using MINITAB.

Flow cell	Mean of slope (hr^{-1})	Standard deviation	R^2	p
1	0.001160	0.001016	0.3950	0.372
2	0.000257	0.000756	0.0540	0.767
3	0.000521	0.000400	0.4600	0.322
4	0.000119	0.000961	0.0080	0.912

The average biofilm density in each flow cell for each replicate during the steady state phase was calculated and plotted in Figure 18. These data were compared between the two replicates as well as among the four flow cells. Figure 18 illustrated that for all the flow cells, the average biofilm density in the replicate 1 was greater than that in the replicate 2. The p values, calculated by two sample t-tests using MINITAB (Table 15), indicated that all the differences were statistically significant. These data indicated a large experiment to experiment variance, which was due to the less control of the experimental conditions such as the treatment of the coverslip surfaces and the pH and temperature of the media.

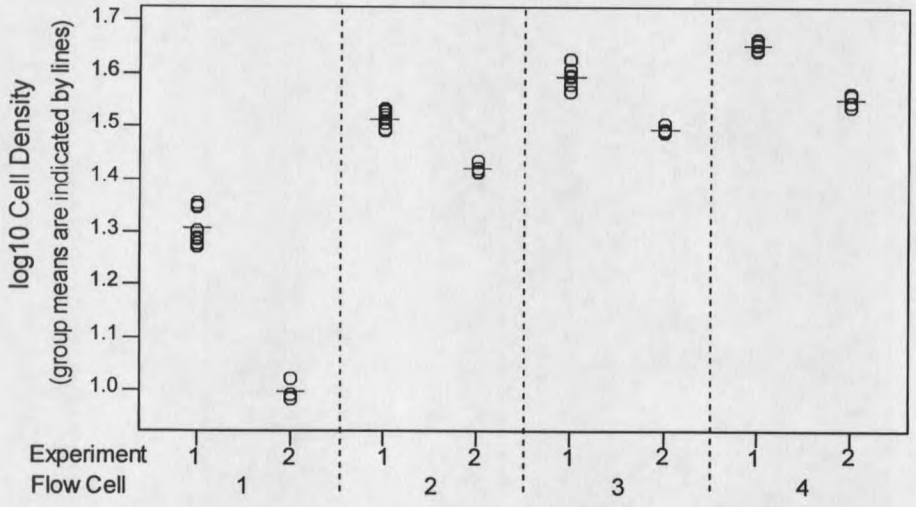

Figure 18. Comparison of the average *Pseudomonas aeruginosa* (PAO1, GFP+) biofilm densities on the coverslip surfaces of four flow cells at the steady state phase before switching the media. The comparison is made between the two replicates as well as among the four flow cells.

Table 15. Comparison of the average *Pseudomonas aeruginosa* (PAO1, GFP+) biofilm densities on the coverslip surfaces of four flow cells between the two replicates. The comparison was made by t-test using MINITAB.

Flow Cells	1	2	3	4
P Values	< 0.001	< 0.001	< 0.001	< 0.001

The average biofilm densities in each flow cell for the two replicates during the steady state phase were calculated and presented in Table 16, along with their standard deviations. These results demonstrated that the order of the biofilm densities in the four flow cells during the steady state phase was flow cell 1 < flow cell 2 < flow cell 3 < flow cell 4.

Table 16. The average *Pseudomonas aeruginosa* (PAO1, GFP+) biofilm densities on the coverslip surfaces of four flow cells. The average densities were calculated for the overall data of the two replicates at the steady state phase before switching the media.

Flow cell	1	2	3	4
Average density of the two experiments	1.2049	1.4836	1.5618	1.6238
Standard deviations	0.1567	0.0487	0.0514	0.0508

The comparisons of the biofilm density among the flow cells during the steady state phase were made by calculating the Fisher's Pairwise Confidence Intervals for each pair of flow cells at $\alpha = 0.05$ level using MINITAB. The results are shown in Table 17.

Table 17 indicated that there were statistically significant differences in biofilm densities among all the flow cells during the steady state phase. This

result, as well as the order of the biofilm densities in the four flow cells, were consistent with the results of the steady state phase in previous research, in which only the flow cell media 1 was used.

Table 17. Comparison of the average *Pseudomonas aeruginosa* (PAO1, GFP+) biofilm densities on the coverslip surfaces among all the flow cells at the steady state phase before switching the media. Presented by the Fisher's Pairwise Confidence Intervals calculated at $\alpha = 0.05$ level using MINITAB. The intervals are for (column level mean) – (row level mean)

Intervals	Flow cell 2	Flow cell 3	Flow cell 4
Flow cell 1	0.2049, 0.3525	0.2831, 0.4306	0.3415, 0.4890
Flow cell 2	---	0.0364, 0.1200	0.0947, 0.1784
Flow cell 3		---	0.0165, 0.1002

Results with Flow Cell Media 2. Both Figure 16 and 17 show that after switching the media, there was significant biofilm accumulation in all the flow cells. This increase contained two continuous phases. At the beginning, there was only a slight increase of biofilm cell numbers in each flow cell, indicating a lag phase. The duration of the lag phase in the second replicate was longer than the first one. This difference was attributed to experiment-to-experiment variation. By the end of the lag phase, a logarithmic growth phase, represented by the last five data points of each flow cell, was observed. The biofilm cell numbers in all of the flow cells increased rapidly during this phase. Cell division was frequently observed, and the cells appeared much brighter (more GFP produced) than before.